Stellar Configurations in $f(R, L_m, T)$ Gravity: Probing Anisotropy and Stability via Minimal Geometric Deformation

M. Zubair^{1,2†} Hira Sohail^{3‡} Saira Waheed^{4§} Amara Ilyas^{5,6,7‡} Irfan Mahmood³

¹Department of Mathematics, COMSATS University Islamabad, Lahore Campus, Lahore, Pakistan ²National Astronomical Observatories, Chinese Academy of Sciences, Beijing 100101, China ³Centre for High Energy Physics, University of the Punjab, 54590, Lahore, Pakistan ⁴Prince Mohammad Bin Fahd University, Al Khobar, Kingdom of Saudi Arabia

⁵Department of Astronomy, School of Physical Sciences, University of Science and Technology of China, Hefei, Anhui 230026, China ⁶CAS Key Laboratory for Researches in Galaxies and Cosmology, University of Science and Technology of China, Hefei, Anhui 230026, China ⁷School of Astronomy and Space Science, University of Science and Technology of China, Hefei, Anhui 230026, China

Abstract: The present study uses the minimal geometric deformation scheme within the paradigm of $f(\mathcal{R}, \mathcal{L}_m, T)$ gravity to model anisotropic compact stars using class-1 embedding spacetime. We introduce deformation of radial component of metric tensor which results in the decoupling of Einstein field equations and introduces an additional gravitational source. The involved constants are then evaluated by adopting the data of seven realistic star candidates through matching of inner region with outer Schwarzschild line element. A comprehensive investigation of three compact stars is done graphically to examine the impact of coupling parameter β and the deformation parameter n, revealing positive well-behaved energy densities and pressures, satisfying energy conditions. The study finds that negative coupling parameter β values allow more mass accumulation while maintaining the crucial physical characteristics such as stability through Herrera's cracking condition and the extended Tolman-Oppenheimer-Volkoff equation. This study emphasizes the importance of gravitational decoupling for mass, redshift and compactness, providing vital insights into the internal structure of stellar bodies within this new generalized gravity framework.

Keywords: Gravitational decoupling, $f(\mathcal{R}, \mathcal{L}_m, T)$ gravity, Minimal geometric deformation

DOI: CSTR:

I. INTRODUCTION

In 1916, Albert Einstein introduced the theory of general relativity (GR) which revolutionized our current understanding of gravitational phenomena and explained various critical astronomical events, including the curvature of spacetime and the formation of stellar as well as galactic structures. One of the most significant predictions of GR is the existence of black holes and compact stellar configurations, all of which result from the gravitational collapse during the eventual stages of a star's life. In 2005, numerous compact objects with high densities were discovered [1]. The theory of GR has continued to demonstrate its accuracy, as evidenced by the precise prediction of gravitational waves by Mercury's perihelion precession, which are recently detected by the Laser Interferometer Gravitational-Wave Observatory and Virgo collaborations [2]. Additionally, the first picture of the shadow of a black hole, captured by the Event Horizon Telescope project, further validated the theory of GR [3]. Despite these remarkable successes, GR has encountered challenges in addressing certain theoretical and observational cosmic issues, such as the unexpected acceleration of cosmos [4–7], non–renormalizability [8], the cosmological constant problem [9], and the mysteries of dark terms of cosmic distribution [10].

To address the limitations of GR, numerous extended gravitational frameworks have been put forwarded in literature. These theories serve as candidates for DE, which is often believed to be a possible source of accelerated cosmic expansion because of its negative pressure. Many of these extended theories involve geometric modifications of GR, providing essential frameworks to support observational cosmic data. For example, $F(\mathcal{R})$ gravity modifies the gravitational theory by introducing a Lagrangian that is a function of the Ricci scalar [11, 12]. An-

Received 30 June 2025; Accepted 9 October 2025

[†] E-mail: mzubairkk@gmail.com; drmzubair@cuilahore.edu.pk

[‡] E-mail: hirasohail02@outlook.com

[§] E-mail: swaheed@pmu.edu.sa

[‡] E-mail: aarks@ustc.edu.cn

[#] E-mail: mahirfan@yahoo.com

^{©2026} Chinese Physical Society and the Institute of High Energy Physics of the Chinese Academy of Sciences and the Institute of Modern Physics of the Chinese Academy of Sciences and IOP Publishing Ltd. All rights, including for text and data mining, AI training, and similar technologies, are reserved.

other significant theory is teleparallel gravity in which the curvature \mathcal{R} is substituted by torsion \mathcal{T} , defined through the Weitzenböck connection in place of the Levi-Civita connection [13, 14]. Initially, this framework was applied to BTZ black hole solutions [15]. Later, it was shown [16] that $F(\mathcal{T})$ theory is fails to comply with the first thermodynamical law of black holes. Examples of other remarkable modified theories of gravity include $f(R, R_{\alpha\beta}^{\alpha\beta}, \Phi)$ [17–19], f(G) gravity [20], $f(\mathcal{R}, \mathcal{T})$ gravity [21], $f(\mathcal{T}, \mathcal{B})$ gravity [22], $f(\mathcal{T}, \mathcal{T})$ [23–26], $f(\mathcal{Q}, \mathcal{T})$ [27, 28] and $f(\mathcal{R}, \mathcal{L}_m)$ theory [29].

A particularly important class of modified theories involves coupling matter and geometry, such as $f(\mathcal{R}, T)$, $f(\mathcal{R}, \mathcal{L}_m)$, and their unification in $f(\mathcal{R}, \mathcal{L}_m, T)$ gravity. These frameworks allow the energy-momentum tensor to influence spacetime geometry directly, leading to richer phenomenology and the emergence of non-conserved matter fields. Recent studies have applied such theories to model anisotropic compact stars, explore deviations in hydrostatic equilibrium, and test energy conditions under strong gravity. Additionally, the Minimal Geometric Deformation (MGD) technique has been increasingly utilized to generate exact or semi-analytical anisotropic solutions within these extended frameworks, demonstrating compatibility with astrophysical observations. These advancements collectively indicate that modified gravity continues to be a fertile ground for addressing outstanding questions in theoretical and observational cosmology. This theory considers the gravitational Lagrangian as a generic function of three fundamental quantities: the Ricci scalar \mathcal{R} , the matter Lagrangian \mathcal{L}_m , and the trace of the energy-momentum tensor T, that is, $\mathcal{L}_{grav} = f(\mathcal{R}, \mathcal{L}_m, T)$ [30–32]. Recent developments have shown that such frameworks can accommodate more realistic compact star models, account for anisotropic matter distributions, and generate modified equilibrium conditions consistent with astrophysical observations. Motivated by these advances, the present study explores anisotropic compact stellar configurations within the $f(\mathcal{R}, \mathcal{L}_m, T)$ gravity framework using the Minimal Geometric Deformation (MGD) technique under the gravitational decoupling approach. This allows us to construct physically viable solutions while incorporating non-minimal matter-geometry coupling that reflect the current direction of research in gravitational modeling.

In recent years, the quest for exact spherically symmetric solutions to the dynamical field equations has become increasingly challenging, primarily due to the presence of numerous non-linear terms, especially in the context of modified gravity theories. A substantial body of literature is available wherein compact star solutions have been constructed under various gravitational frameworks. Nashed and El Hanafy [33] investigated spherically symmetric dynamical configurations in f(R) gravity using a quadratic model defined by $f(R) = R + \epsilon R^2$. For the interi-

or spacetime geometry, they adopted the Krori-Barua metric and considered anisotropic matter distributions. Utilizing observational data of PSR J0740+6620 from NICER and XMM-Newton observations, they determined viable values of the parameter ϵ and demonstrated that the resulting structure is stable and satisfies all essential physical conditions. Extending this study, Nashed and Capozziello [34] employed an exponential model, $f(\mathcal{R}) = \mathcal{R}e^{\zeta\mathcal{R}}$, in combination with observational data from the pulsar SAX J1748.9-2021, yielding significant results. In another investigation, Nashed [35] obtained exact solutions for anisotropic, perfect-fluid spheres within the $f(\mathcal{R},T)$ framework, adopting a linear form of the function as $f(\mathcal{R},T) = \mathcal{R} + \beta T$, where β is a dimensional parameter. The resulting solutions were found to be in hydrostatic equilibrium, with all relevant physical quantities expressed in terms of β and the compactness parameter $C = \frac{2GM}{Rc^2}$. Within the same theoretical context, the author further derived solutions by introducing specific assumptions on anisotropy as well as radial metric component, leading to compelling physical conclusions.

In the framework of conformal $f(\mathcal{R},T)$ gravity, the modeling of compact stars has been explored by Das et al. [36], where solutions were generated to describe the interior geometry of compact objects by employing a barotropic equation of state (EoS). A detailed graphical analysis demonstrated that the obtained solutions are physically consistent and correspond to radiating compact stars. Kumar et al. [37] constructed stellar models with isotropic matter distributions in curvature-matter coupled gravity, assuming a linear functional form of $f(\mathcal{R},T)$. Their analysis confirmed the stability of the proposed configuration through various physical criteria. The pursuit of anisotropic and non-singular compact star models was further carried out in [38], where the barotropic EoS was applied within the $f(\mathcal{R},T)$ framework. The results indicated that the energy conditions are satisfied and the models exhibit stable behavior. In another recent study [39], compact stellar configurations were investigated by employing the Krori-Barua metric as the interior geometry within the context of $\kappa(\mathcal{R}, T)$ gravity. Utilizing observational data from three compact stars —4U 1820–30, SAX J1808.4–3658, and Her X–1—the physical acceptability and stability of the models were examined through graphical methods.

The technique of gravitational decoupling through Minimal Geometric Deformation (MGD) offers a novel strategy that facilitates the derivation of acceptable solutions for spherically relativistic configurations. This method introduces various new elements that contribute to the pursuit of solutions for spherically symmetric objects by incorporating more complex gravitational sources into the existing energy-momentum tensor while preserving spherical symmetry. The MGD approach was

first presented by Ovalle within the framework of the Randall-Sundrum brane-world scenario [40, 41]. It was later extended to deform the standard Schwarzschild solution [42], leading to the formulation of new black hole models [43]. Initial applications of this technique were primarily developed in the context of brane-world models [44, 45], black hole acoustics [46], and studies on the Generalized Uncertainty Principle (GUP) and Hawking radiation involving fermions [47]. Additionally, it was applied to purely anisotropic matter distributions [48, 49] and the anisotropic Einstein-Maxwell system [50, 51]. Subsequently, this technique has been employed in various theories, such as in [52], where the MGD approach was used to extend the Buchdahl solution, and in [53], where it was applied to obtain an anisotropic static BTZ model in a (2+1)-dimensional spacetime. Other applications can also be found in the literature [54–56], and particularly, within the context of $f(\mathcal{R},T)$ theory, one can see references given in [57, 58]. In the context of F(R,T) theory, researchers [59] have modeled some new anisotropic compact stars based on decoupling approach. For achieving this target, they have assumed linear choice of F(R,T) function, a well-known ansatz for metric potential namely modified Durgapal-Fuloria model and Pseudo-Isothermal dark matter as a new source to the anisotropic seed solution. It was seen that the obtained solution is non-singular and agrees with all necessary physical conditions. In the context of GR, authors [60] adopted the decoupling method to focus on the strange star model, and it is argued that through mass-radius analysis conducted for neutron star mergers and huge pulsars, the model parameters can be effectively constrained. It is concluded that their outcomes exceeded the observed masses of compact stars and also showed a correlation of recent findings from gravitational wave events like GW190814 and GW200210.

Following the work of Nashed et al. [33-35], the primary target of present paper is to utilize the radii and masses of some known pulsars located within globular clusters and constrain different involved model parameters. By performing graphical analysis, we will try to assess whether the proposed MGD-based model in realm of $f(R, L_m, T)$ gravity remains physically valid for the observed compact star candidates with known radii and masses. To this end, we shall select some well-known stars and test our model against their properties. Specifically, we shall perform the complete physical analysis (including energy conditions, stability, etc.) for one representative star. For other known stars, we will include the relevant numerical results in tabular form to show how the values of different parameters (c, B, A) vary under different configurations which further can change the behavior of all physical properties. This dual approach allows us to validate the model across multiple realistic scenari-

We construct anisotropic compact star models within the framework of $f(\mathcal{R}, \mathcal{L}_m, T)$ gravity using the gravitational decoupling approach via Minimal Geometric Deformation (MGD) and embedding class-I spacetime. By deforming the radial metric component, the field equations are decoupled into isotropic and anisotropic sectors, enabling the construction of physically viable models consistent with observed stellar data. This work aims to explore how the generalized theory, which unifies previous models such as $f(\mathcal{R}, T)$ and $f(\mathcal{R}, \mathcal{L}_m)$, influences the key physical features of compact stars like stability, energy conditions, and mass-radius behavior. The manuscript is organized as follows: Section II outlines the theoretical framework of this modified gravity; Section III discusses the metric and matching conditions; Section IV presents the detailed physical analysis; and Section V concludes our main findings.

II. BASICS OF $f(\mathcal{R}, \mathcal{L}_m, T)$ THEORY

Since our primary objective is to study compact star models beyond the paradigm of GR, specifically within the framework of $f(\mathcal{R}, \mathcal{L}_m, T)$ theory, this section provides an overview of the fundamental mathematical structure of this modified gravity theory, along with the necessary assumptions needed to achieve the outlined goal. Haghani and Harko proposed [30] a novel framework that unifies both the $f(\mathcal{R}, T)$ and $f(\mathcal{R}, \mathcal{L}_m)$ theories. This innovative approach leads to a new Lagrangian density incorporating the Ricci scalar, the trace of the energy-momentum tensor, and the Lagrangian of ordinary matter, defined by the following gravitational action:

$$S = \frac{1}{16\pi} \int f(\mathcal{R}, \mathcal{L}_m, T) \sqrt{-g} d^4 x + \int \mathcal{L}_m \sqrt{-g} d^4 x$$
$$+\beta \int \mathcal{L}_{\theta} \sqrt{-g} d^4 x. \tag{1}$$

Herein, $f(\mathcal{R}, \mathcal{L}_m, T)$ is a generic function of geometrical and gravitational quantities, and thus leads to the violation of the principle of minimal interaction between matter and geometry [30]. Consequently, unlike to GR, the dynamical equations can no longer be written in the conventional form where *spacetime geometry equals ordinary matter*, and hence the standard conservation of energy-momentum tensor is not guaranteed. Furthermore, the quantities \mathcal{L}_m and \mathcal{L}_{ϑ} correspond to the matter sector and an additional gravitational source sector (commonly referred to as the ϑ -sector), respectively. A dimensionless constant β , representing the coupling parameter, is introduced. In the metric formalism, variation of the action with respect to $g^{\mu\nu}$ yields the following field equations:

$$f_{\mathcal{R}}\mathcal{R}_{\mu\nu} - \frac{1}{2}[f - (f_{\mathcal{L}} + 2f_T)\mathcal{L}_m]g_{\mu\nu} + (g_{\mu\nu}\Box - \nabla_{\mu}\nabla_{\nu})f_{\mathcal{R}}$$

$$= \left[8\pi G + \frac{1}{2}(f_{\mathcal{L}} + 2f_T)\right]T_{\mu\nu} + 8\pi G\beta\vartheta_{\mu\nu} + f_T\tau_{\mu\nu}, \tag{2}$$

where $f_{\mathcal{R}} = \partial f/\partial \mathcal{R}$, $f_T = \partial f/\partial T$, $f_{\mathcal{L}} = \partial f/\partial \mathcal{L}$ and $\Box = g^{\mu\nu}\nabla_{\mu}\nabla_{\nu}$. Here the covariant derivative is symbolized by ∇_{ν} . Further, the terms $T_{\mu\nu}$, the extra source $\vartheta_{\mu\nu}$ and $\tau_{\mu\nu}$ are, respectively, given as follow

$$T_{uv} = g_{uv} \mathcal{L}_m - 2\partial \mathcal{L}_m / \partial g^{\mu v}, \tag{3}$$

$$\vartheta_{\mu\nu} = g_{\mu\nu} \mathcal{L}_{\vartheta} - 2\partial \mathcal{L}_{\vartheta} / \partial g^{\mu\nu}, \tag{4}$$

$$\tau_{\mu\nu} = g^{\alpha\beta} \delta T_{\alpha\beta} / \delta g^{\mu\nu}. \tag{5}$$

Equation (2) can be re-arranged as follows

$$G_{\mu\nu} = \frac{1}{f_{\mathcal{R}}} \left[(8\pi G + (f_T + \frac{1}{2}f_{\mathcal{L}}))T_{\mu\nu} + \frac{1}{2}(f - \mathcal{R}f_{\mathcal{R}})g_{\mu\nu} - (f_T + \frac{1}{2}f_{\mathcal{L}})\mathcal{L}_m g_{\mu\nu} + (\nabla_{\mu}\nabla_{\nu} - g_{\mu\nu}\Box)f_{\mathcal{R}} + f_T \tau_{\mu\nu} \right].$$
 (6)

In this setup, we assume the spherically symmetric metric written in below form:

$$ds^{2} = -e^{v(r)}dt^{2} + e^{\xi(r)}dr^{2} + r^{2}(d\theta^{2} + \sin^{2}\theta d\phi^{2}).$$
 (7)

The distribution of stellar matter is assumed to be an anisotropic fluid, which is defined by the following equation:

$$T_{uv} = (\rho + p_t)V_uV_v + p_t g_{uv} + (p_r - p_t)\chi_u \chi_v,$$
 (8)

where ρ is energy density, p_r is radial while p_t denotes the transverse stress. The four velocity is symbolized by V_{α} and χ_{α} to be the radial four vector satisfying:

$$V^{u} = e^{\frac{-v}{2}} \delta_{0}^{u}, \quad V^{u} V_{u} = 1, \quad \chi^{u} = e^{\frac{-a}{2}} \delta_{1}^{u}, \quad \chi^{u} \chi_{u} = -1.$$

For the sake of simplicity in equations (6), we shall assume the well-motivated forms of Lagrangian matter \mathcal{L}_m and $f(\mathcal{R}, \mathcal{L}_m, T)$ function. In this study, we suppose the Lagrangian matter form as $\mathcal{L}_m = (p_r + 2p_t)/3$. Also, we assume a simple form of $f(\mathcal{R}, \mathcal{L}_m, T)$ function which is given by

$$f(\mathcal{R}, \mathcal{L}_m, T) = \mathcal{R} + \gamma T + \lambda \mathcal{L}_m, \tag{9}$$

where γ and λ are coupling constants. The primary reason for choosing this model (9) is that it results in a minimal coupling between matter and geometry, avoiding the complications of high order derivatives and enabling the successful implementation of either the MGD or e-MGD scheme. Earlier research has also employed similar functional forms to produce regular and physically feasible stellar models, such as in f(R,T) [61] and $f(R,L_m)$ grav-While there are fewer examples in $f(R, L_m, T)$ gravity where it was demonstrated to preserve central regularity and enable a physically consistent anisotropic extension, our work expands on this strategy and demonstrates that it is still efficient and consistent in this larger context. Interestingly, since the model (9) is linear in all variables, i.e., \mathcal{R} , \mathcal{L}_m and T, therefore the right hand side of Eq.(6) is similar to the one obtained in GR theory as $f_{\mathcal{R}} = 1$. Contrarily, on the left hand side, quantities \mathcal{L}_m and T alter the anisotropic fluid distribution via the dimension-less interaction constants. Introducing this form of $f(\mathcal{R}, \mathcal{L}_m, T)$ in Eq.(6), one can obtain the following generic expression:

$$G_{\mu\nu} = 8\pi G T_{\mu\nu} + 8\pi G \beta \vartheta_{\mu\nu} + \left(\gamma + \frac{\lambda}{2}\right) T_{\mu\nu} + \frac{1}{2} (\gamma T + \lambda \mathcal{L}_m) g_{\mu\nu} - \left(\gamma + \frac{\lambda}{2}\right) \mathcal{L}_m g_{\mu\nu}.$$
(10)

III. MGD AND EMBEDDING CLASS-I SPACE TIME

In this part, we will introduce the concept of minimal geometric deformation, which introduces anisotropy into the set of field equations. This method incorporates an additional gravitational source, $\vartheta_{\mu\nu}$, into the energy-momentum tensor through gravitational decoupling. We introduce the following transformation:

$$e^{\nu(r)} \longrightarrow e^{H(r)} + \beta \quad \eta(r),$$
 (11)

$$e^{-\xi(r)} \longrightarrow e^{-W(r)} + \beta \quad \psi(r).$$
 (12)

Here, the notations $\eta(r)$ and $\psi(r)$ denote the deformation functions introduced for the temporal and radial components of the spacetime metric, respectively. According to the MGD approach, one of these functions can be set to zero, i.e., either $\eta(r) = 0$ or $\psi(r) = 0$. In this study, we choose $\eta(r) = 0$, thereby introducing deformation exclusively in the radial component. The constant β serves as a free coupling parameter, and by setting $\beta = 0$, the original field equations of $f(\mathcal{R}, \mathcal{L}_m, T)$ gravity are recovered. Based on this framework, the resulting deformed function is expressed as follows

$$e^{-\xi(r)} \longrightarrow e^{-W(r)} + \beta \psi(r).$$
 (13)

Now, we introduce the additional gravitational source $\vartheta_{\mu\nu}$ into the original energy-momentum tensor, resulting in the effective energy-momentum tensor for $f(\mathcal{R}, \mathcal{L}_m, T)$ gravity. The standard dynamical equations, expressed in terms of MGD, can then be written as

$$\mathcal{R}_{\mu\nu} - \frac{1}{2} \mathcal{R} g_{\mu\nu} = 8\pi G T_{\mu\nu}^{eff}, \tag{14}$$

where

$$T_{\mu\nu}^{eff} = 8\pi G \hat{T}_{\mu\nu} + 8\pi G \beta \vartheta_{\mu\nu} = 8\pi G T_{\mu\nu} + \left(\gamma + \frac{\lambda}{2}\right) T_{\mu\nu} + \frac{1}{2} \left(\gamma T + \lambda \mathcal{L}_m\right) g_{\mu\nu} - \left(\gamma + \frac{\lambda}{2}\right) \mathcal{L}_m g_{\mu\nu} + 8\pi G \beta \vartheta_{\mu\nu}.$$

$$(15)$$

Here, the original energy-momentum tensor is given by $T_{\mu\nu} = {\rm diag}(\rho, -p_r, -p_t, -p_t)$, while the additional gravitational source is represented as $\vartheta_{\mu\nu} = {\rm diag}(\vartheta_0^0, \vartheta_1^1, \vartheta_2^2, \vartheta_3^3)$. The components of $\vartheta_{\mu\nu}$ introduce anisotropies into the self-gravitating system, thereby transforming the field equations into a set of quasi-Einstein field equations. This transformation is achieved through the deformation of the metric, and the resulting expressions for the effective energy density and pressures under gravitational decoupling are obtained as follows:

$$\rho^{eff} = \hat{\rho} + \beta \vartheta_0^0, \quad p_r^{eff} = \hat{p}_r - \beta \vartheta_1^1, \quad p_t^{eff} = \hat{p}_t - \beta \vartheta_2^2, \quad (16)$$

with

$$\hat{\rho} = 8\pi G \rho + \frac{1}{2} (3\gamma + \lambda) \rho - \frac{\gamma}{6} p_r - \frac{\gamma}{3} p_t, \tag{17}$$

$$\hat{p}_r = 8\pi G p_r - \frac{\gamma}{2} \rho + \left(\frac{7\gamma}{6} + \frac{\lambda}{2}\right) p_r + \frac{\gamma}{3} p_t, \tag{18}$$

$$\hat{p}_t = 8\pi G p_t - \frac{\gamma}{2} \rho + \frac{\gamma}{6} p_r + \left(\frac{4\gamma}{3} + \frac{\lambda}{2}\right) p_t. \tag{19}$$

The anisotropy parameter is defined as

$$\Delta = \frac{r}{2}(p_t^{eff} - p_r^{eff}) = \Delta + \Delta_{\theta}, \tag{20}$$

These relations effectively decouple the original dynamical equations into two distinct systems: one governing the seed isotropic matter distribution and the other characterizing the new anisotropic configuration arising due to gravitational decoupling. By substituting Eq. (13) into the field equations (17)–(19), two separate sets of equations can be obtained, where $\Delta = \frac{r}{2}(p_t - p_r)$ and $\Delta_\theta = \frac{r}{2}\beta(\theta_1^1 - \theta_2^2)$. The first system corresponds to the standard field equations governed by the energy-momentum tensor $T_{\mu\nu}$ in the limit $\beta = 0$, and is supplemented by a conservation equation. These governing equations are expressed as follows:

$$\rho = \left(e^{-a(r)} \left(ra'(r)(16\gamma + 96\pi G + 6\lambda - \gamma rv'(r)) + 2\left(e^{a(r)} - 1\right)(8\gamma + 48\pi G + 3\lambda) + 2\gamma r^2 v''(r) + \gamma r^2 v'(r)^2 + 4\gamma rv'(r)\right)\right) / \left(3r^2(2\gamma + 16\pi G + \lambda)(4\gamma + 16\pi G + \lambda)\right),$$
(21)

$$p_{r} = \left(e^{-a(r)}\left(\gamma r a'(r)(r v'(r) + 8) - 2\left(\left(e^{a(r)} - 1\right)(8\gamma + 48\pi G + 3\lambda) + \gamma r^{2}v''(r)\right) + 2r(10\gamma + 48\pi G + 3\lambda)v'(r) + \gamma\left(-r^{2}\right)v'(r)^{2}\right)\right) / \left(3r^{2}(2\gamma + 16\pi G + \lambda)(4\gamma + 16\pi G + \lambda)\right),$$
(22)

$$p_{t} = \left(e^{-a(r)}\left(-ra'(r)(8\gamma + r(10\gamma + 48\pi G + 3\lambda)v'(r) + 96\pi G + 6\lambda) + 2\gamma\left(8e^{a(r)} + 5r^{2}\left(2v''(r) + v'(r)^{2}\right) + 8rv'(r) - 8\right) + 3r(16\pi G + \lambda)\left(2rv''(r) + rv'(r)^{2} + 2v'(r)\right)\right)\right)\left(6r^{2}(2\gamma + 16\pi G + \lambda)(4\gamma + 16\pi G + \lambda)\right)$$
(23)

and the conservation equation is given by

$$-\frac{dp_{r}}{dr} - \frac{H(r)'}{2}(\rho + p_{r}) + \frac{2(p_{t} - p_{r})}{r} + \frac{d}{dr} \left[\frac{\gamma}{6(8\pi G + \gamma + \lambda/2)} (3\rho - p_{r} - 2p_{t}) \right] = 0.$$
 (24)

The spacetime solution for the aforementioned set of equations can be expressed by the below metric:

$$ds^{2} = e^{H(r)}dt^{2} - e^{W(r)}dr^{2} - r^{2}(d\theta^{2} + \sin^{2}\theta d\varphi^{2}).$$
 (25)

The quasi-Einstein equations are the second set of equations, which apply to the source $\vartheta_{\mu\nu}$. These are derived by using the relationships defined by Eq.(16) and the deformed metric supplied in Eq.(13), where $\beta \neq 0$. The resulting quasi-Einstein equations, along with the conservation equation, are described as below

$$\vartheta_{0}^{0} = \left(r\psi'(r)(\gamma r H'(r) - 2(8\gamma + 48\pi G + 3\lambda)) + \psi(r)(\gamma r (2rH''(r) + H'(r)(rH'(r) + 4)) - 2(8\gamma + 48\pi G + 3\lambda)) \right) /$$

$$\left(3r^{2}(2\gamma + 16\pi G + \lambda)(4\gamma + 16\pi G + \lambda) \right),$$
(26)

$$\vartheta_{1}^{1} = \left(\gamma r (rH'(r) + 8) \psi'(r) - \psi(r) \left(16\gamma + r(H'(r)(20\gamma + 96\pi G - \gamma rH'(r) + 6\lambda) - 2\gamma rH''(r) \right) + 96\pi G + 6\lambda \right) \right) /$$

$$\left(3r^{2}(2\gamma + 16\pi G + \lambda)(4\gamma + 16\pi G + \lambda) \right),$$
(27)

$$\vartheta_{2}^{2} = -\left(r\psi'(r)(8\gamma + r(10\gamma + 48\pi G + 3\lambda)H'(r) + 96\pi G + 6\lambda) + \psi(r)\left(r\left(2r(10\gamma + 48\pi G + 3\lambda)H''(r) + H'(r)(16\gamma + r(10\gamma + 48\pi G + 3\lambda)H'(r) + 96\pi G + 6\lambda)\right) - 16\gamma\right)\right) / \left(6r^{2}(2\gamma + 16\pi G + \lambda)(4\gamma + 16\pi G + \lambda)\right), \tag{28}$$

$$-\frac{H(r)'}{2}(\vartheta_0^0 - \vartheta_1^1) - \frac{d\vartheta_1^1}{dr} + \frac{2}{r}(\vartheta_2^2 - \vartheta_1^1) + \frac{d}{dr} \left[\frac{\gamma}{6(8\pi G + \gamma + \lambda/2)} \left(3\vartheta_0^0 + \vartheta_1^1 + 2\vartheta_2^2 \right) \right] = 0.$$
 (29)

At this juncture, it is pertinent to note that two sets of equations are decoupled, exhibiting no exchange of energy between them and interacting solely through gravitational effects.

A. Class-I Solutions and Minimal Geometric Deformation Scheme

To solve the two sets of field equations involving unknown functions W(r) and H(r), we select a metric potential that meets the key criteria: it must be finite, monotonically increasing with r, and reach a minimum at r=0, ensuring regularity. These conditions, as outlined in [63], are essential for deriving physically viable static spherically symmetric perfect fluid solutions. In this work, we adopt the following form for the metric potential, which satisfies the necessary mathematical conditions and facilitates the derivation of physically viable expressions for the effective energy density and pressures. The chosen

metric potential is given by

$$e^{W} = 1 + cr^{2}e^{nar^{2}}, (30)$$

where c, n, and a are arbitrary constants. This specific form has been widely utilized as an ansatz, particularly in the construction of class-I solutions [64, 65]. It is interesting to mention here that this metric is consistent with the criteria of being regular at the center, exhibiting monotonically increasing trend with minimum at r = 0, and $e^W = 1 + O(r^2)$. Therefore, it is a valid choice to consider for modeling of compact stars within this theory. For a spacetime to be categorized under embedding class-I, it is imperative that Eq.(25) satisfies the Karmarkar condition, originally formulated by Karmarkar in 1948 [66]. This condition is expressed as

$$\mathcal{R}_{1414} = \frac{\mathcal{R}_{1212}\mathcal{R}_{3434} + \mathcal{R}_{1224}\mathcal{R}_{1334}}{\mathcal{R}_{2323}}.$$
 (31)

By incorporating the condition specified in Eq.(31), and given that $R_{2323} \neq 0$ as noted in [67], we derive the following equation that establishes a relationship between the two spacetime functions W(r) and H(r), as outlined below

$$\frac{W'H'}{1 - e^W} = W'H' - 2H'' - H'^2, \tag{32}$$

where $e^{W(r)} \neq 1$. By integrating the first equation, we derive the subsequent equation, which illustrates the manner in which the four-dimensional spacetime, as described by Eq.(31), is embedded within a five-dimensional pseudo-Euclidean space. This corresponds to solutions of embedding class-I. It is defined as

$$e^{H(r)} = \left(\mathbb{A} + \mathbb{B} \int \sqrt{e^{W(r)} - 1} \, dr\right)^2,\tag{33}$$

where \mathbb{A} and \mathbb{B} are constants due to integration. Substituting Eq.(30) into the above equation permits us to determine the value of the metric $e^{H(r)}$, as provided below

$$e^{H(r)} = \left(\mathbb{A} + \frac{\mathbb{B}\sqrt{cr^2e^{anr^2}}}{anr} \right)^2. \tag{34}$$

The constants \mathbb{A} , \mathbb{B} , and c can be evaluated through the application of the matching condition. In the subsequent section, we will fix the constants λ and a. It is noted that the metric potential $e^{H(r)}$ is a radial dependent monotonically increasing function and exhibits positive, finite, and regular trend with $e^{H(r)} \to 1$ as $r \to 0$, thus ensuring the absence of singularities. Therefore, this metric potential is suitable for modeling a relativistic compact object within the framework of $f(\mathcal{R}, T, \mathcal{L}_m)$ gravity via MGD approach. Below line element can then be used to describe the field equations given by Eqs.(21) through (23):

$$ds^{2} = -\left(\mathbb{A} + \frac{\mathbb{B}\sqrt{cr^{2}e^{anr^{2}}}}{anr}\right)^{2}dt^{2} + \left(1 + cr^{2}e^{nar^{2}}\right)^{-1}dr^{2} + r^{2}\left(d\theta^{2} + \sin^{2}\theta d\phi^{2}\right). \tag{35}$$

To obtain the complete solutions for our model, it is necessary to calculate the components of $\vartheta_{\mu\nu}$. This requires determining the deformation function $\psi(r)$. Several methods can be employed to find $\psi(r)$, including:

• Mimicking the density constraint $(\vartheta_0^0 = \rho)$;

- Mimicking the pressure constraint $(\vartheta_1^1 = p_r)$;
- Relating the components of $\vartheta_{\mu\nu}$ through various equations of state, such as polytropic, barotropic, or linear equations.

However, the determination of deformation function $\psi(r)$ often becomes mathematically intricate, especially when aiming to maintain physical acceptability and analytic solvability. To address this, we adopt a deformation function that is free from singularities, exhibits a non-decreasing behavior, and has been extensively utilized in previous studies for constructing physically viable anisotropic models [68–70]. The chosen form is not arbitrary; it is carefully selected to be fully compatible with the prescribed seed solution, ensuring that the resulting field equations remain analytically tractable and physically consistent. While alternative functional forms for $\psi(r)$ are theoretically permissible, they frequently introduce significant non-linearities or yield unphysical features, such as singularities or negative pressures. Moreover, the selected function has also been successfully employed in conjunction with the same seed metric in earlier works, further justifying its use in the present analysis. This form is given by

$$\psi(r) = \frac{ncr^2}{cr^2 + 1}.\tag{36}$$

The complete spacetime structure related to the energy-momentum tensor $T_{\mu\nu}^{eff}$ can be explicitly defined as follows

$$ds^{2} = -\left(\mathbb{A} + \frac{\mathbb{B}\sqrt{cr^{2}e^{anr^{2}}}}{anr}\right)^{2}dt^{2} + \left(\frac{(1+cr^{2}e^{nar^{2}})(cr^{2}+1)}{(cr^{2}+1)+\beta ncr^{2}(1+cr^{2}e^{nar^{2}})}\right)dr^{2} + r^{2}\left(d\theta^{2} + \sin^{2}\theta d\phi^{2}\right),$$
(37)

where

$$e^{\nu(r)} = \left(\mathbb{A} + \frac{\mathbb{B}\sqrt{cr^2e^{anr^2}}}{anr}\right)^2,\tag{38}$$

$$e^{-\xi(r)} = \frac{(1+cr^2e^{nar^2})(cr^2+1)}{(cr^2+1)+\beta ncr^2(1+cr^2e^{nar^2})}.$$
 (39)

In the subsequent computations, below characterization of total state quantities, i.e., the energy density, radial and tangential pressures will be implemented:

$$\rho^{\text{(total)}} = \rho + \alpha \vartheta_0^0, \tag{40}$$

$$p_r^{(\text{total})} = p_r - \alpha \vartheta_1^1, \tag{41}$$

$$p_t^{\text{(total)}} = p_t - \alpha \vartheta_2^2, \tag{42}$$

where density and pressures are provided by Eqs.(21)-(23). These relations involve additional geometric quantities which are interacted via coupling parameter α .

The quantities $\rho^{\text{(total)}}$, along with $p_r^{\text{(total)}}$ and $p_t^{\text{(total)}}$ for completing the system, can be expressed as follows

$$\begin{split} \rho^{\text{total}} &= \frac{1}{3k_1 r^2 (2\gamma + k_1)} \left(\frac{1}{k_2 r + 1} \left(\frac{4a^2 \mathbb{B}^2 \gamma k_2^2 n^2 r^4}{k_3^2} + \frac{4a \mathbb{B} \gamma n (k_2 r)^{3/2} \left(a \mathbb{A} n r \left(a n r^2 + 1 \right) + \mathbb{B} \sqrt{k_2 r} \right)}{k_3^2} \right. \\ &+ \frac{2a \mathbb{B} \gamma k_2 n r^2 \left(\frac{2a n r^2 + 2}{k_2 r + 1} - 2a n r^2 + 2 \right)}{k_3} + \frac{4k_2 r \left(a n r^2 + 1 \right) \left(8\gamma + 48\pi G + 3\lambda t \right)}{k_2 r + 1} + 2k_2 r (8\gamma + 48\pi G + 3\lambda t)} \\ &+ \frac{2\beta c n r^2}{\left(c r^2 + 1 \right)^2} \left(\left(k_2 \left(-a^2 \mathbb{A}^2 n^2 r (8\gamma + 3\lambda t) \left(c r^2 + 3 \right) + 2a \mathbb{B} n \sqrt{k_2 r} \left(y \left(r^2 \left(c \right) \left(a n r^2 \left(a n r^2 + 3 \right) - 8 \right) \right) \right. \right. \\ &+ \left. \left. \left(a n r^2 + 4 \right) \right) - 24 \right) - 3\lambda \left(c r^2 + 3 \right) \right) + \mathbb{B}^2 k_2 \left(2\gamma \left(r^2 \left(a n r^2 + 4 \right) \left(a c n r^2 \right) \right) \right) \\ &+ \left. \left. \left(a n r^2 + 4 \right) \right) - 24 \right) - 3\lambda \left(c r^2 + 3 \right) \right) \right) / \left(k_3^2 \right) + 48\pi G \left(c r^2 + 3 \right) \right) \right), \\ p_r^{\text{total}} &= \frac{1}{3k_1 r^2 \left(2\gamma + k_1 \right)} \left(\frac{1}{k_2 r + 1} \left(-\frac{4a^2 \mathbb{B}^2 \gamma k_2^2 n^2 r^2}{k_3^2} - \frac{4a \mathbb{B} \gamma n \left(k_2 r \right)^{3/2} \left(a \mathbb{A} n r \left(a n r^2 + 1 \right) + \mathbb{B} \sqrt{k_2 r} \right)}{k_3^2} \right. \\ &+ \frac{2a \mathbb{B} k_2 n r^2 \left(2\gamma \left(-\frac{a n r^2 + 1}{k_2 r + 1} + a n r^2 + 11 \right) + 96\pi G + 6\lambda \right)}{k_3} + \frac{16\gamma k_2 r \left(a n r^2 + 1 \right)}{k_2 r + 1} - 2k_2 r (8\gamma \right)}{k_3} \\ &+ \frac{48\pi G + 3\lambda t}{k_3} \right) + \left(\beta c n r^2 \left(\left(2\left(a \mathbb{A} n \left(c r^2 + 1 \right) \sqrt{k_2 r} \left(8\gamma + 48\pi G + 3\lambda \right) + \mathbb{B} k_2 \left(48\pi G \left(c r^2 + 1 \right) \left(2a n r^2 + 1 \right) \right) \right)}{k_2 r + 1} \right) \\ &+ 2\gamma \left(r^2 \left(c \left(a n r^2 \left(9 - a n r^2 \right) + 4 \right) + a n \left(8 - a n r^2 \right) \right) + 4 \right) + 3\lambda \left(c r^2 + 1 \right) \left(2a n r^2 + 1 \right) \right) \right) / (k_3) - 16\gamma \right) \right) \\ &- \left(\left((c r^2 + 1)^2 \right) \right), \\ &+ \frac{2}{3k_1} \left(\frac{2}{2\gamma k_1} \left(\left(\frac{2}{2} r e^{2n^2} \left(a^2 k_2 n^2 \left(-48G \left(\pi a n r^2 + \pi \right) + r^2 \left(\frac{4\gamma k_2}{r} - a n \left(4\gamma + 3\lambda \right) \right) - 3\lambda \right) \right) \right. \\ &+ \frac{2}{4B} \left(\frac{k_2}{r} \left(\frac{4}{2\gamma k_2} \left(\frac{k_2}{r} \left(\frac{4}{2\gamma k_2} \left(\frac{k_2}{r} \left(\frac{2}{r} \right) + a n \left(8\pi G \left(a n r^2 + 2 \right) + a n r^2 \left(10\gamma + 3\lambda \right) + 6 \left(3\gamma + \lambda \right) \right) + 8\gamma k_2^2 \right) \right. \\ &+ \frac{2}{3k_1} \left(\frac{k_2}{r} \left(\frac{k_2}{r} \left(\frac{k_2}{r} \left(\frac{k_2}{r} \left(\frac{k_2}{r} \right) + a n \left(8\pi G \left(a n r^2 + 2 \right) + a n r^2 \left(10\gamma + 3\lambda \right) + 6 \left($$

where

$$k_1 = s2\gamma + 16\pi G + \lambda$$
, $k_2 = cre^{anr^2}$, $k_3 = aAn \sqrt{k_2r} + Bk_2$.

B. Boundary Conditions and Determination of Constants: Israel-Darmois Matching

Matching conditions are crucial for understanding the physical characteristics of any gravitational model by aligning the interior and exterior geometries across a hypersurface. This process is governed by two primary conditions:

- Continuity of metric coefficients: The metric components of both spacetimes must be continuous at the hypersurface. This constraint ensures that there is no discontinuity in the metric across the boundary.
- Extrinsic curvature matching: The extrinsic curvature of both spacetimes must be equal at the hypersurface. This requirement, further, leads to the condition: $p_r^{\text{eff}} = 0$, which means that there is no difference in the tensor components of the stress energy across the boundary.

These conditions are essential for ensuring a smooth transition and consistency across the interior and exterior geometries of any gravitational model. For this study, we choose the exterior Schwarzschild spacetime as given below

$$ds^{2} = -\left(1 - \frac{2\mathcal{M}}{r}\right)dt^{2} + \left(1 - \frac{2\mathcal{M}}{r}\right)^{-1}dr^{2} + r^{2}\left(d\theta^{2} + \sin^{2}\theta d\phi^{2}\right). \tag{44}$$

By equating the above exterior spacetime metric with Eq.(37) and applying the continuity conditions for the metric potentials, we derive the following two relations:

$$e^{\nu(r)} = 1 - \frac{2\mathcal{M}}{\mathcal{R}},\tag{45}$$

$$e^{-\xi(r)} = 1 - \frac{2\mathcal{M}}{\mathcal{R}},\tag{46}$$

where the terms \mathcal{M} and \mathcal{R} , respectively, refer to total mass and radius of the compact star. The second form of continuity, in which the pressure vanishes at the boundary and hence allows stability in a true vacuum, is presented below:

$$p_r^{total}(r)|_{r=\mathcal{R}} = \left(p_r - \alpha \vartheta_1^1\right)|_{r=\mathcal{R}} = 0. \tag{47}$$

By utilizing Eqs.(45)-(47) and re-arranging them with the appropriate substitutions, the values of the random constants \mathbb{A} , \mathbb{B} , and c can be found as follows

$$\begin{split} \mathbb{A} &= -\frac{\mathrm{B}\,\sqrt{\mathrm{c}\mathcal{R}^{2}}e^{\mathrm{a}n^{s}\mathcal{R}^{2}}}{\mathrm{a}n\mathcal{R}}, \\ \mathbb{B} &= \left(\left(\mathrm{c}\,\sqrt{\mathcal{R}}\,\sqrt{\mathcal{R}-2\mathcal{M}}\left(\mathrm{c}\mathcal{R}^{2}e^{2\mathrm{a}n\mathcal{R}^{2}}\left(8\gamma\left(\beta\mathrm{c}^{2}n\mathcal{R}^{4}-\left(\mathrm{c}\mathcal{R}^{2}+1\right)^{2}\right)+48\pi G\left(\mathrm{c}\mathcal{R}^{2}+1\right)\left(\mathrm{c}\mathcal{R}^{2}(\beta n-1)-1\right)\right) \\ &+ 3\lambda\left(\mathrm{c}\mathcal{R}^{2}+1\right)\left(\mathrm{c}\mathcal{R}^{2}(\beta n-1)-1\right)\right)+e^{\mathrm{a}n\mathcal{R}^{2}}\left(8\mathrm{a}\gamma n\left(\mathrm{c}\mathcal{R}^{3}+\mathcal{R}\right)^{2}+16\beta\gamma\mathrm{c}^{2}n\mathcal{R}^{4}+48\pi G\left(\mathrm{c}\mathcal{R}^{2}+1\right)\right. \\ &\left. \left. \left(\mathrm{c}\mathcal{R}^{2}(2\beta n-1)-1\right)+3\lambda\left(\mathrm{c}\mathcal{R}^{2}+1\right)\left(\mathrm{c}\mathcal{R}^{2}(2\beta n-1)-1\right)\right)+\beta n\left(48G\left(\pi\mathrm{c}\mathcal{R}^{2}+\pi\right)+\mathrm{c}\mathcal{R}^{2}(8\gamma+3\lambda)+3\lambda\right)\right)\right) \\ &\left. \left. \left(2\sqrt{\mathcal{C}}\mathcal{R}^{2}e^{\mathrm{a}n\mathcal{R}^{2}}\left(\gamma\left(\mathcal{R}^{2}\left(\mathrm{c}\left(\beta\mathrm{c}^{2}n\mathcal{R}^{4}e^{2\mathrm{a}n\mathcal{R}^{2}}\right)\right)+\mathrm{a}n\right)-8\right)+\mathrm{c}\mathcal{R}^{2}(\beta n+1)\left(\mathrm{a}n\mathcal{R}^{2}-9\right)\right. \\ &\left. +2e^{\mathrm{a}n\mathcal{R}^{2}}\left(\beta\mathrm{c}n\mathcal{R}^{2}\left(\mathcal{R}^{2}\left(\mathrm{c}\left(\mathrm{a}n\mathcal{R}^{2}-9\right)+\mathrm{a}n\right)-8\right)-5\left(\mathrm{c}\mathcal{R}^{2}+1\right)^{2}\right)+\mathrm{a}n\mathcal{R}^{2}(\beta n+2)-8\beta n-18\right)+\mathrm{a}n\right)-9\right) \\ &\left. -48\pi G\left(\mathrm{c}\mathcal{R}^{2}+1\right)\left(\mathrm{c}\mathcal{R}^{2}e^{\mathrm{a}n\mathcal{R}^{2}}+1\right)\left(\mathrm{c}\mathcal{R}^{2}\left(\beta n\left(\mathrm{c}\mathcal{R}^{2}e^{\mathrm{a}n\mathcal{R}^{2}}+1\right)+1\right)+1\right)+1\right)-3\lambda\left(\mathrm{c}\mathcal{R}^{2}+1\right) \\ &\left. \left(\mathrm{c}\mathcal{R}^{2}e^{\mathrm{a}n\mathcal{R}^{2}}+1\right)\left(\mathrm{c}\mathcal{R}^{2}\left(\beta n\left(\mathrm{c}\mathcal{R}^{2}e^{\mathrm{a}n\mathcal{R}^{2}}+1\right)+1\right)+1\right)+1\right)\right)\right)\right), \\ c &= \left(4\mathcal{M}\right)/\left(-2\mathcal{M}\mathcal{R}^{2}\left(e^{\mathrm{a}n\mathcal{R}^{2}}+1\right)+\sqrt{\mathcal{R}^{4}\left(\left(-(\mathcal{R}-2\mathcal{M})e^{\mathrm{a}n\mathcal{R}^{2}}+2\mathcal{M}+\beta n\mathcal{R}\right)^{2}-8\mathcal{M}e^{\mathrm{a}n\mathcal{R}^{2}}(2\mathcal{M}+\mathcal{R}(\beta n-1))\right)}\right) \\ &+\mathcal{R}^{3}\left(e^{\mathrm{a}n\mathcal{R}^{2}}-\beta n\right)\right). \end{aligned}$$

Random constants \mathbb{A} , \mathbb{B} , and c are then evaluated by taking $\beta = 0.2$ and $\beta = -0.2$, and the summary of resulting values is provided in Tables 1 and 2 where the data of seven selected stellar models has been utilized. In both

instances, the fixed parameters are: $\lambda = 1 \times 10^{-12}$, a = 0.03, and $\gamma = 0.009$, while the coupling parameter can assume any non-zero real value, as illustrated in the tables.

Table 1. Synopsis of computed values of constants based on the data of seven stellar candidates for MGD case $(\beta = 0.2, \lambda = 1 * 10^{-12}, a = 0.03, \gamma = 0.009)$.

Star Models	Mass $\mathcal{M}/\mathcal{M}_{\odot}$	Radius $\mathcal{R}(km)$	Mass-radius($\frac{M}{R}$)	С	\mathbb{B}	A
Her X-1 [71]	0.85±0.15	8.1±0.41	0.154	0.00339865	-0.0279575	-0.289412
LMC X-4 [72]	1.04 ± 0.09	8.301±0.2	0.184	0.00403809	-0.029791	-0.165948
Cen X-3 [73]	1.49 ± 0.08	9.178±0.13	0.239	0.00454612	-0.0306402	-0.0403881
4U 1608-52 [74]	1.74±0.14	9.528±0.15	0.269	0.0049576	-0.03128	0.0445229
Vela X-1 [75]	1.77±0.08	9.56 ± 0.08	0.273	0.00502456	-0.0312868	0.057035
PSR J1614-2230 [76]	1.97±0.04	9.69±0.2	0.300	0.0056665	-0.0324197	0.166191
PSR J0740+6620 [77]	2.07±0.04	12.34±0.2	0.247	0.00214646	-0.02322001	-0.3364949

Table 2. Synopsis of computed values of constants based on the data of seven star models for MGD case $(\beta = -0.2, \lambda = 1 * 10^{-12}, a = 0.03, \gamma = 0.009)$.

Star Models	Mass $\mathcal{M}/\mathcal{M}_{\odot}$	Radius $\mathcal{R}(km)$	Mass-radius($\frac{M}{R}$)	С	B	A
Her X-1 [71]	0.85±0.15	8.1±0.41	0.154	0.00325493	-0.028568	-0.289414
LMC X-4 [72]	1.04 ± 0.09	8.301±0.2	0.184	0.0038583	-0.0304771	-0.165951
Cen X-3 [73]	1.49 ± 0.08	9.178 ± 0.13	0.239	0.00432607	-0.0314096	-0.0403919
4U 1608-52 [74]	1.74 ± 0.14	9.528±0.15	0.269	0.00470364	-0.0321131	0.0445179
Vela X-1 [75]	1.77±0.08	9.56±0.08	0.273	0.00476514	-0.0322297	0.0570297
PSR J1614-2230 [76]	1.97±0.04	9.69±0.2	0.300	0.00535511	-0.0333488	0.166184
PSR J0740+6620 [77]	2.07±0.04	12.34±0.2	0.247	0.00205513	-0.0237099	-0.364951

Utilizing the listed constant values for the selected stellar candidates, we have generated the plots of the metric potentials in Figures (1(a)) and (1(b)). These figures illustrate the trend of the metric potentials as functions of the radial coordinate r for two distinct constant values across four different stellar models. In both cases, the metric potentials exhibit regular, monotonically increasing, and finite behavior throughout the stellar interior, without any indication of singularities.

IV. PHYSICAL ANALYSIS

In this part, we will analyze the stability of our solutions by exploring various physical characteristics that are crucial for validity as well as stability of celestial objects in any gravitational framework. This include the illustration of energy density, pressures (p_r, p_t) , and their gradients, anisotropy, velocities, equation of state (EoS), mass, compactness, and redshift. All of these measures will be explained in detail in the following subsections.

A. Energy Density, Pressures and Gradients

In self-gravitating bodies, particularly highly dense objects such as compact objects, the matter components including energy density and pressures are anticipated to exhibit a specific conduct. The energy density and pressures are expected to be maximum at the core of the star

showing finite, positive, and singularities free behavior which decrease towards the surface. This behavior supports the stability of the model within the theoretical framework proposed. Figures (2) and (3) illustrate the radial profiles of energy density, as well as tangential and radial pressures, throughout the radius of the compact star models. It is noticed that the tangential pressure vanishes at the boundary. Furthermore, we have analyzed the gradients of energy density and pressures, which are essential for the construction of a compact star model. It is argued [78] that these gradients must exhibit negative behavior. We have conducted this analysis by taking two specific cases: first, by varying the parameter n while keeping the coupling parameter β constant, and second, by varying β while maintaining a constant value for n. This examination ensures the consistency of our model with the below conditions under both scenarios:

$$\frac{d\rho}{dr} < 0; \quad \frac{dp_r}{dr} < 0; \quad \frac{dp_t}{dr} < 0 \tag{49}$$

Figures (3(b)) and (3(c)) illustrate the behavior of all gradients under both scenarios. It is observed that the gradients are in accordance with the essential conditions, exhibit a decreasing trend, and vanish at the stellar core, i.e., at r = 0. This behavior is consistent with the physical expectations for a compact star model, where the energy

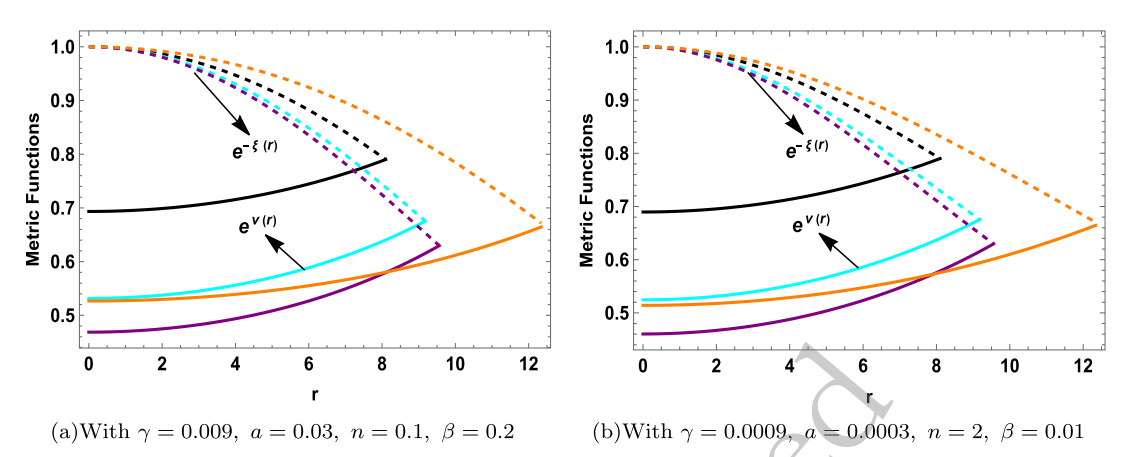


Fig. 1. (color online) For the compact star Her X-1 ($\mathcal{M}/\mathcal{M}_{\odot} = 0.85$, $\mathcal{R} = 8.1$)(\blacksquare), Cen X-3 ($\mathcal{M}/\mathcal{M}_{\odot} = 1.49$, $\mathcal{R} = 9.178$)(\blacksquare), Vela X-1 ($\mathcal{M}/\mathcal{M}_{\odot} = 1.77$, $\mathcal{R} = 9.56$)(\blacksquare) and PSR J0740+6620 ($\mathcal{M}/\mathcal{M}_{\odot} = 2.07$, $\mathcal{R} = 12.34$)(\blacksquare), the variations in metric functions against r are shown. All plots use $\lambda = 1 \times 10^{-12}$.

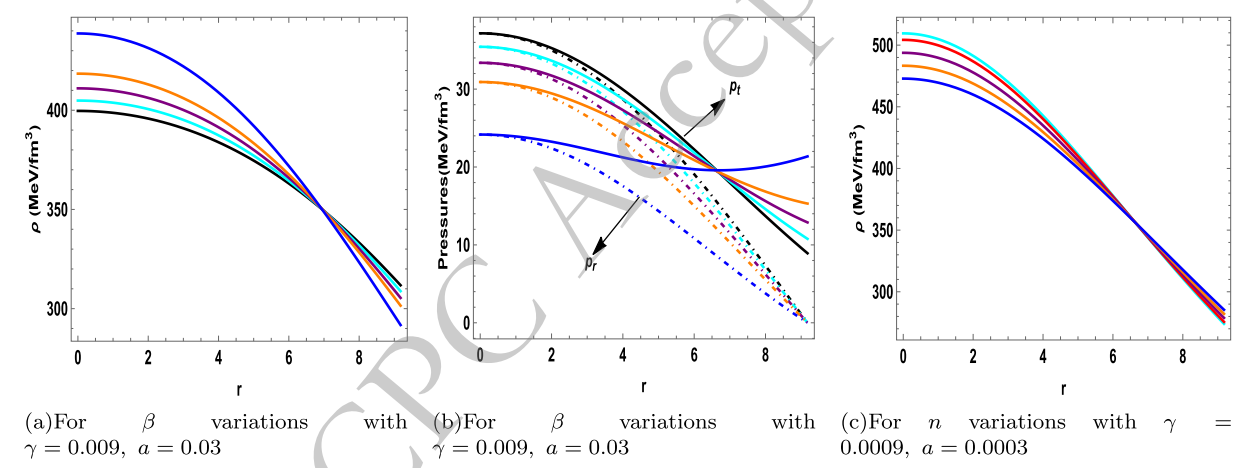


Fig. 2. (color online) For the compact star Cen X-3 ($\mathcal{M}/\mathcal{M}_{\odot} = 1.49$, $\mathcal{R} = 9.178$), the variations in energy density and pressures with the radial coordinate r are shown. Subfigures (a) and (b) depict energy density and pressures (p_t & p_r) for n = 0.1 with $\beta = 0$ (\blacksquare), $\beta = 0.5$ (\blacksquare), $\beta = 1.5$ (\blacksquare), and $\beta = 2.5$ (\blacksquare). Subfigure (c) shows energy density for $\beta = 0.01$ with n = 0.5 (\blacksquare), n = 1 (\blacksquare), n = 2 (\blacksquare), and n = 4 (\blacksquare). All plots use $\lambda = 1 \times 10^{-12}$.

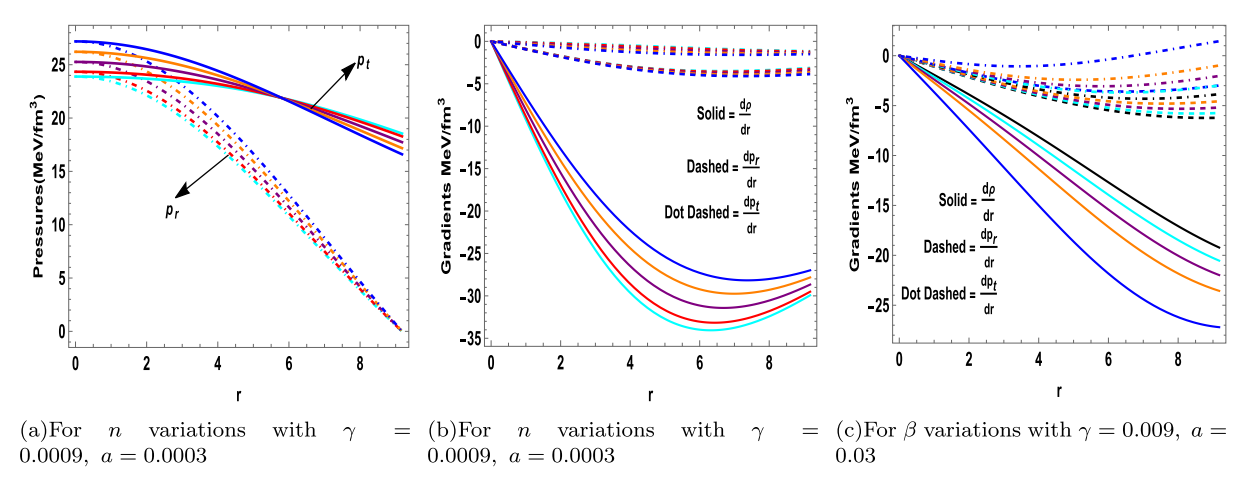


Fig. 3. (color online) For the compact star Cen X-3 ($\mathcal{M}/\mathcal{M}_{\odot} = 1.49$, $\mathcal{R} = 9.178$), the variations in pressures and gradients with the radial coordinate r are shown. Subfigures (a) and (b) depict pressures (p_t & p_r) and gradients for $\beta = 0.01$ with n = 0.5 (\blacksquare), n = 1 (\blacksquare), n = 2 (\blacksquare), and n = 4 (\blacksquare), Subfigure (c) shows gradients for n = 0.1 with $\beta = 0$ (\blacksquare), $\beta = 0.5$ (\blacksquare), $\beta = 1$ (\blacksquare), $\beta = 1.5$ (\blacksquare), and $\beta = 2.5$ (\blacksquare). All plots use $\lambda = 1 \times 10^{-12}$.

density and pressures reach their maximum at the center and decrease outwards.

$$\left. \frac{d\rho}{dr} \right|_{r=0} = 0; \quad \left. \frac{dp_r}{dr} \right|_{r=0} = 0; \quad \left. \frac{dp_t}{dr} \right|_{r=0} = 0 \tag{50}$$

B. Anisotropy, Energy Conditions and Equilibrium Forces

Pressure anisotropy is a crucial factor in assessing the stability of a compact obejct, as it provides valuable insights into the interior stellar structure. For a stable compact star, the anisotropy denoted by Δ , should be nonzero. When the tangential pressure p_t exceeds the radial pressure p_r , the anisotropy Δ is positive ($\Delta > 0$) and exhibits a repulsive (outward-directed) force. Conversely, if p_r is greater than p_t , the anisotropy is negative ($\Delta < 0$)

and refers to an attractive (inward-directed) force [79]. Figures (4(c)) and (5(c)) demonstrate the behavior of anisotropy as a function of radius. It is found that anisotropy is zero at the core and becomes positive, increasing towards the boundary in both cases as shown graphically. This trend confirms the repulsive trend of anisotropy and the necessary anti-gravitational behavior of the anisotropic force for maintaining the stability of stellar structures.

Energy conditions represent some mathematical constraints on the energy-momentum tensor of self-gravitating bodies and form the root cause of singularity theorems [80] as well as entropy bounds [81]. These conditions are pivotal in assessing the feasibility of a relativistically stable model. The primary energy conditions include the strong energy condition (SEC), weak energy condition (WEC), null energy condition (NEC), and dominant energy condition (DEC). Mathematically, these are provided as below:

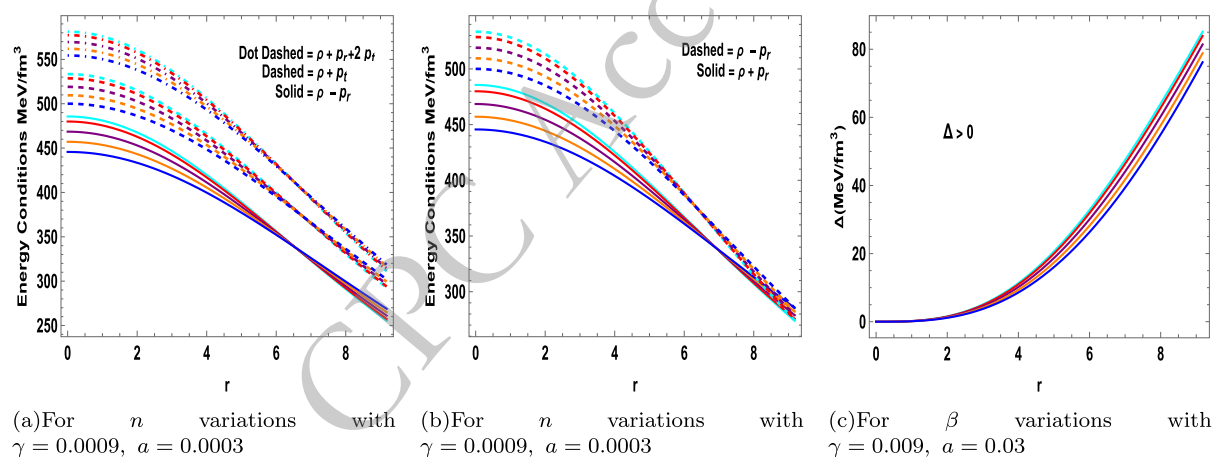


Fig. 4. (color online) For the compact star Cen X-3 ($\mathcal{M}/\mathcal{M}_{\odot} = 1.49$, $\mathcal{R} = 9.178$), the variations in energy conditions and anisotropy with the radial coordinate r are shown. Subfigures (a) and (b) depict energy conditions and (c) depict anisotropy for $\beta = 0.01$ with n = 0.5 (\blacksquare), n = 1 (\blacksquare), n = 2 (\blacksquare), n = 3 (\blacksquare), and n = 4 (\blacksquare). All plots use $\lambda = 1 \times 10^{-12}$.

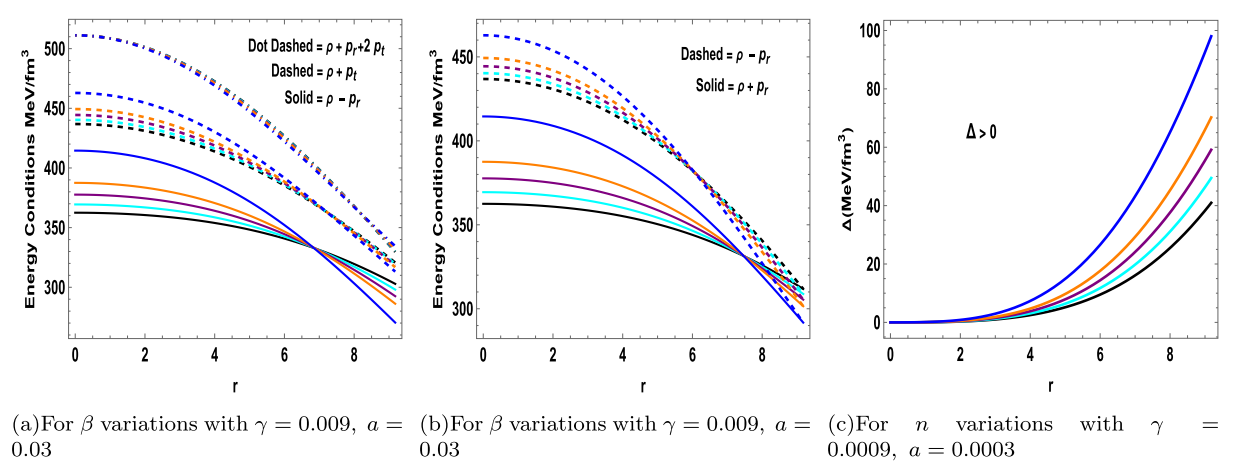


Fig. 5. (color online) For the compact star Cen X-3 ($\mathcal{M}/\mathcal{M}_{\odot} = 1.49$, $\mathcal{R} = 9.178$), the variations in energy conditions and anisotropy with the radial coordinate r are shown. Subfigures (a) and (b) depict energy conditions and (c) depict anisotropy for n = 0.1 with $\beta = 0$ (\blacksquare), $\beta = 0.5$ (\blacksquare), $\beta = 1.5$ (\blacksquare), and $\beta = 2.5$ (\blacksquare). All plots use $\lambda = 1 \times 10^{-12}$.

$$\begin{aligned} \mathbf{NEC} : \rho^{eff} &\geq 0, \\ \mathbf{WEC} : \rho^{eff} + p_t^{eff} &\geq 0, \qquad \qquad \rho^{eff} + p_r^{eff} &\geq 0. \\ \mathbf{SEC} : \rho^{eff} + 2p_t^{eff} + p_r^{eff} &\geq 0, \\ \mathbf{DEC} : \rho^{eff} - |p_r^{eff}| &\geq 0, \qquad \qquad \rho^{eff} - |p_t^{eff}| &\geq 0. \end{aligned} \tag{51}$$

For a physically captivating model, the associated inequalities must be satisfied, ensuring that these energy conditions reach their maximum at the core of the star and remain positive throughout its structure. As showed in Figures (4(a)), (4(b)), (5(a)) and (5(b)), all specified

energy conditions are met under both scenarios: when varying the parameter n while keeping the coupling parameter β constant, and when varying β while maintaining n constant. This consistency across both cases further validates the stability of presented models.

Next, we analyze the equilibrium conditions through the involved forces namely the gravitational force (F_g) , the hydrostatic force (F_h) , the anisotropic force (F_a) and the modified force (F_m) due to our modified $f(\mathcal{R}, T, \mathcal{L}_m)$ gravity model. By incorporating the effects of the MGD approach, the extended Tolman-Oppenheimer-Volkoff (TOV) equation for our model is formulated as follows

$$-\underbrace{\frac{H(r)'}{2}\left[\rho+p_r+\beta(\vartheta_0^0-\vartheta_1^1)\right]}_{F_g} -\underbrace{\left(\frac{dp_r}{dr}-\beta\frac{d\vartheta_1^1}{dr}\right)}_{F_h} +\underbrace{\frac{2}{r}\left[p_r-p_r-\beta(\vartheta_0^0-\vartheta_1^1)\right]}_{F_a} +\underbrace{\frac{d}{dr}\left[\frac{\gamma}{6(8\pi G+\gamma+\lambda/2)}\left((3\rho-p_r-2p_t)+\beta(3\vartheta_0^0+\vartheta_1^1+2\vartheta_2^2)\right]\right)}_{F_m} = 0.$$
(52)

To ensure the stability of our model within $f(\mathcal{R}, T, \mathcal{L}_m)$ gravity, the total impact of all forces, i.e., gravitational (F_g) , hydrostatic (F_h) , anisotropic (F_a) , and the modified force (F_m) , must be zero, indicating that these forces are in equilibrium. This balancing effect ensures the stability of any configuration. Figures 6(a) and 6(b) demonstrate the behavior of these forces in two distinct scenarios. In the first scenario, the parameters are held constant while the forces are plotted as functions of varying n as depicted in Figure 6(a). The figure shows

that the gravitational force is counteracted by the combined hydrostatic and anisotropic forces, which act in the opposite direction. This equilibrium prevents the gravitational collapse, while the modified force remains constant and exerts only a small impact on the hydrostatic balance. In the second scenario, the forces are plotted for varying values of the coupling parameter β as illustrated in Figure 6(b). This figure confirms that even with different values of β , all forces balance each other, further affirming the stability of our model. These findings valid-

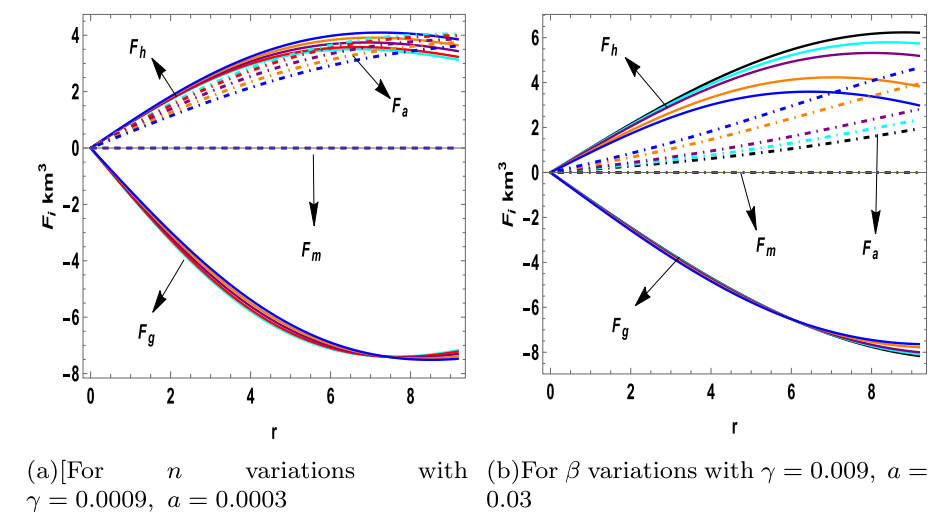


Fig. 6. (color online) For the compact star Cen X-3 ($\mathcal{M}/\mathcal{M}_{\odot} = 1.49$, $\mathcal{R} = 9.178$), the variations in forces with the radial coordinate r are shown. Subfigures (a) depict forces for $\beta = 0.01$ with n = 0.5 (\blacksquare), n = 1 (\blacksquare), n = 2 (\blacksquare), n = 3 (\blacksquare), and n = 4 (\blacksquare), Subfigure (b) shows forces for n = 0.1 with $\beta = 0$ (\blacksquare), $\beta = 0.5$ (\blacksquare), $\beta = 1$ (\blacksquare), $\beta = 1.5$ (\blacksquare), and $\beta = 2.5$ (\blacksquare). All plots use $\lambda = 1 \times 10^{-12}$.

ate that our model is not only stable but also represents a physically viable relativistic system.

C. Equation of state and stability analysis

Equation of state represents a dimensionless constraint on the parameters governing the radial and tangential pressures. These limitations play a pivotal role in establishing the relationship between state variables as expressed by the following equation:

$$\omega_t = \frac{p_t}{\rho}, \quad \omega_r = \frac{p_r}{\rho}.$$
 (53)

It is argued that both these parameters must lie between 0 and 1 to ensure the physical stability of a relativistic model and confirm the non-exotic nature of the internal fluid distribution [82]. Figures 7(a) and 7(b) depict the trend of these parameters along the radial direction, with ω_r vanishing at the star's boundary for two scenarios: varying n and varying β , as labeled in the figures. The results clearly demonstrate that both EoS parameters fall within the aforementioned limits, thereby confirming that the solutions are physically viable and consistent referring to stable relativistic star models.

To evaluate the physical stability of anisotropic compact star models, the pressure components must be constrained by the speed of light [83]. This is achieved using Herrera's concept of cracking [84], which defines the expressions for tangential and radial velocities, as outlined below. Both velocities must lie within the range [0,1], a requirement termed as the causality condition.

$$v_r^2 = \frac{dp_r}{d\rho}, \quad v_t^2 = \frac{dp_t}{d\rho}.$$
 (54)

The concept of cracking has been further extended by Abreu [85] and Andreasson [86] to assess the stability of stellar structures. This extension is represented by the following equations and inequalities. For a model to be physically promising and potentially stable, it must adhere the conditions outlined below

$$= \begin{cases} -1 \le v_t^2 - v_r^2 \le 0 & \text{Potentially stable} \\ 0 < v_t^2 - v_r^2 \le 1 & \text{Potentially unstable} \end{cases}$$
 (55)

Figures (8(a)), (8(b)), (8(c)), and (9(a)) illustrate the radial and tangential velocities (v_r^2 and v_t^2) and their differences. As shown, the velocities remain within the specified regions for both scenarios: varying β and varying n, which confirm the stability of our models. These results reinforce the physical viability and consistency of the model, further validating its capacity to represent a stable relativistic system.

D. Adiabatic Index

The adiabatic index, which describes the stiffness of the EoS by measuring the change in pressure in response to slight variations in matter density, is a critical factor in analyzing the stability of stellar structures, both relativistically and non-relativistically. Chandrasekhar noted in his paper [87] that the adiabatic index should adhere to $\Gamma > 4/3$, a criterion that has been extensively examined by various authors for both isotropic and anisotropic stellar models [88, 89]. The adiabatic index corresponding to the radial and tangential components is provided below

$$\Gamma_r = \frac{\rho + p_r}{p_r} \left(\frac{dp_r}{d\rho} \right) = \frac{\rho + p_r}{p_r} v_r^2 \tag{56}$$

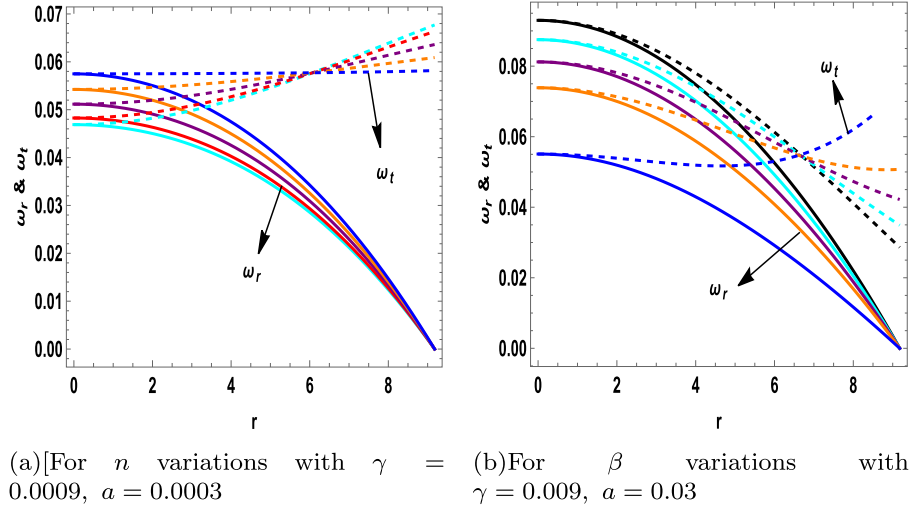


Fig. 7. (color online) For the compact star Cen X-3 ($M/M_{\odot} = 1.49$, $\mathcal{R} = 9.178$), the variations in EoS with the radial coordinate r are shown. Subfigures (a) EoS(w_t & w_r) for $\beta = 0.01$ with n = 0.5 (\blacksquare), n = 1 (\blacksquare), n = 2 (\blacksquare), n = 3 (\blacksquare), and n = 4 (\blacksquare), Subfigure (b) shows EoS(w_t & w_r) for n = 0.1 with $\beta = 0$ (\blacksquare), $\beta = 0.5$ (\blacksquare), $\beta = 1.5$ (\blacksquare), and $\beta = 2.5$ (\blacksquare). All plots use $\lambda = 1 \times 10^{-12}$.

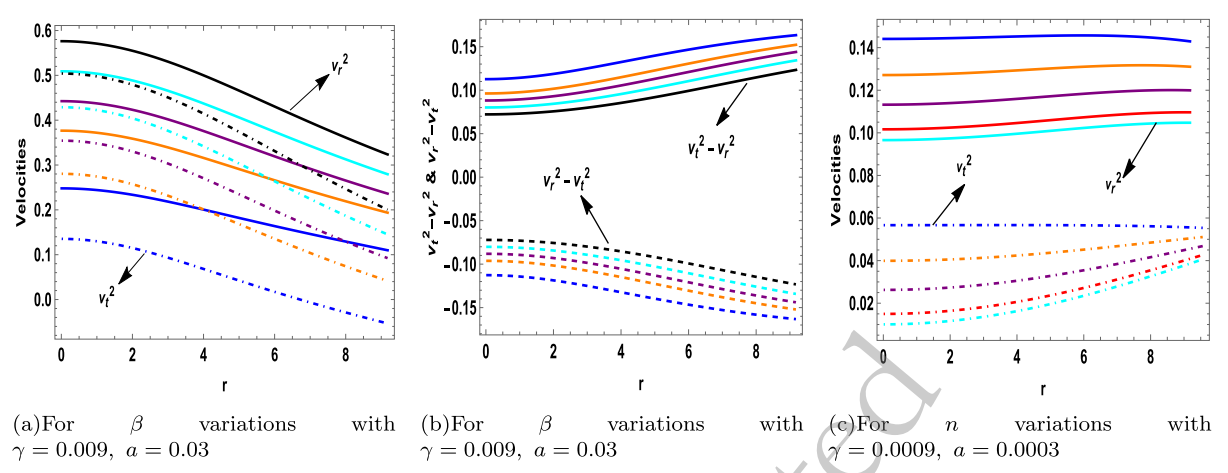


Fig. 8. (color online) For the compact star Cen X-3 ($\mathcal{M}/\mathcal{M}_{\odot} = 1.49$, $\mathcal{R} = 9.178$), the variations in velocities and velocities difference with the radial coordinate r are shown. Subfigures (a) and (b) depict velocities ($v_t^2 \& v_r^2$) and velocities difference ($v_t^2 - v_r^2 \& v_r^2 - v_t^2$) for n = 0.1 with $\beta = 0$ (\blacksquare), $\beta = 0.5$ (\blacksquare), $\beta = 1$ (\blacksquare), $\beta = 1.5$ (\blacksquare), and $\beta = 2.5$ (\blacksquare). Subfigure (c) shows velocities ($v_t^2 \& v_r^2$) for $\beta = 0.01$ with n = 0.5 (\blacksquare), n = 1 (\blacksquare), n = 2 (\blacksquare), n = 3 (\blacksquare), and n = 4 (\blacksquare). All plots use $\lambda = 1 \times 10^{-12}$.

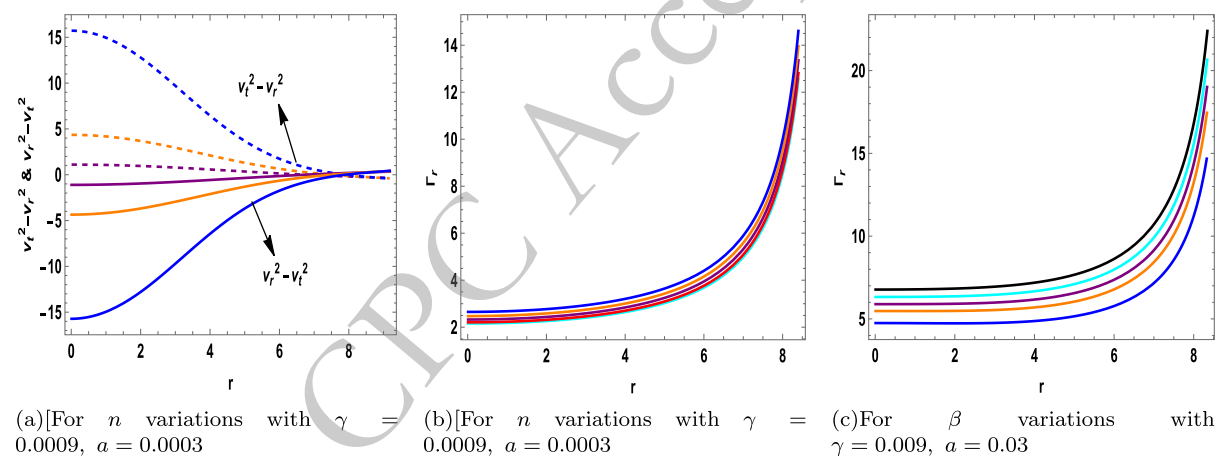


Fig. 9. (color online) For the compact star Cen X-3 ($\mathcal{M}/\mathcal{M}_{\odot} = 1.49$, $\mathcal{R} = 9.178$), the variations in velocities difference and adiabatic index (Γ_r) with the radial coordinate r are shown. Subfigures (a) and (b) depict the velocities difference ($v_t^2 - v_r^2 \& v_r^2 - v_t^2$) and adiabatic index for $\beta = 0.01$ with n = 0.5 (\blacksquare), n = 1 (\blacksquare), n = 2 (\blacksquare), n = 3 (\blacksquare), and n = 4 (\blacksquare), Subfigure (c) shows adiabtic index for n = 0.1 with $\beta = 0$ (\blacksquare), $\beta = 0.5$ (\blacksquare), $\beta = 1.5$ (\blacksquare), and $\beta = 2.5$ (\blacksquare). All plots use $\lambda = 1 \times 10^{-12}$.

$$\Gamma_t = \frac{\rho + p_t}{p_t} \left(\frac{dp_t}{d\rho} \right) = \frac{\rho + p_t}{p_t} v_t^2. \tag{57}$$

Figures (9(b)) and (9(c)) illustrate the conduct of the adiabatic index Γ_r , demonstrating that its value consistently exceeds 4/3 in both scenarios when varying β and varying n. This result confirms the stability of the model under these conditions. The adiabatic index Γ_t is not plotted, as this index does not lead to any significant physical insight in this context. Additionally, Moustakidis [90] discusses the critical value of the adiabatic index Γ , emphasizing its strong dependence on the mass-to-radius ratio $(\mathcal{M}/\mathcal{R})$. As shown below, the critical values of Γ for seven different stellar candidates are provided in Tables 3 and 4. In these tables, it can be observed that for all stellar candidates, $\Gamma_{\rm crit}$ exceeds 4/3. The calculation of $\Gamma_{\rm crit}$

incorporates the modified mass resulting from gravitational decoupling. These findings further affirm the stability and physical consistency of our models.

$$\Gamma_{crit} = \frac{4}{3} + \frac{19}{42} \frac{2M}{\mathcal{R}}.$$
 (58)

E. Mass function, compactness factor and redshift function

In this section, we will talk about the inter-connection between the mass function, compactness, and redshift, as these quantities are inherently related. It is a well-famed result that mass function must exhibit positive increasing behavior and consistent with the radial coordinate limit, i.e., $r \to 0$, $\mathbb{M}(r) \to 0$. The mass reaches its

PSR J0740+6620 [77]

1 55469

$(\beta = 0.2, \pi = 1 * 10^{\circ}, u = 0.2)$	- 0.05, 7 - 0.002	·)·						
Star objects	M_0/\mathcal{M}_{\odot}	$\mathcal{R}(km)$	$u_0 = M_0/\mathcal{R}$	z_s	M/\mathcal{M}_{\odot}	$u = M/\mathcal{R}$	$z_s(MGD)$	$\Gamma_{crit}(MGD)$
Her X-1 [71]	0.85	8.1	0.155	0.203153	0.839975	0.152772	0.19999	1.47156
LMC X-4 [72]	1.04	8.301	0.185	0.259026	1.02773	0.182395	0.254704	1.49836
Cen X-3 [73]	1.49	9.178	0.239	0.384532	1.47275	0.236397	0.377241	1.54722
4U 1608-52 [74]	1.74	9.528	0.269	0.471337	1.71993	0.265932	0.461549	1.57394
Vela X-1 [75]	1.77	9.56	0.278	0.483339	1.74958	0.269611	0.473173	1.57727
PSR J1614-2230 [76]	1.97	9.69	0.300	0.579186	1.94716	0.296032	0.565684	1.60117

Table 3. Synopsis of total mass along with compactness factor values by utilizing the MGD contribution for parameters $(\beta = 0.2, \lambda = 1 * 10^{-12}, a = 0.03, \gamma = 0.009)$.

Table 4. Synopsis of total mass along with compactness parameter values by taking the MGD contribution for parameters $(\beta = -0.2, \lambda = 1 * 10^{-12}, a = 0.03, \gamma = 0.009)$.

0.406152

2.04937

0.244662

0.399352

0.247

Star objects	M_0/\mathcal{M}_\odot	$\mathcal{R}(km)$	$u_0 = M_0/\mathcal{R}$	z_s	M/\mathcal{M}_{\odot}	$u = M/\mathcal{R}$	$z_s(MGD)$	$\Gamma_{crit}(MGD)$
Her X-1 [71]	0.85	8.1	0.155	0.203153	0.859676	0.156355	0.206229	1.4748
LMC X-4 [72]	1.04	8.301	0.185	0.259026	1.05183	0.186672	0.263238	1.50223
Cen X-3 [73]	1.49	9.178	0.239	0.384532	1.50664	0.241837	0.391676	1.55214
4U 1608-52 [74]	1.74	9.528	0.269	0.471337	1.75935	0.272028	0.480962	1.57945
Vela X-1 [75]	1.77	9.56	0.278	0.483339	1.78969	0.275792	0.493341	1.58286
PSR J1614-2230 [76]	1.97	9.69	0.300	0.579186	1.99201	0.302851	0.59253	1.60734
PSR J0740+6620 [77]	2.07	12.34	0.247	0.406152	2.08997	0.249509	0.412826	1.55908

maximum value at the boundary when $r = \mathcal{R}$. However, as previously discussed, gravitational decoupling introduces an additional gravitational source, which influences the mass function. Therefore, the modified mass function for the current theory is given by

2.07

12.34

$$\mathbb{M}(r) = 4\pi \int_0^r \rho^{eff}(r_1) r_1^2 dr_1 = 4\pi \int_0^r [\rho(r_1) + \beta \vartheta_0^0(r_1)] r_1^2 dr_1$$
(59)

or

$$\mathbb{M}(r) = \frac{r}{2} \left(1 - e^{-a(r)} \right) = \frac{r}{2} \left(1 - e^{-W(r)} - \beta \psi(r) \right). \tag{60}$$

This modification to the mass relation reflects the impact of the supplemental gravitational contributions resulting from the decoupling process, which further affects the structure and dynamics of the compact object. The revised equation can be expressed as follows, with the first component representing the mass at $r = \mathcal{R}$ derived solely from $f(\mathcal{R}, \mathcal{L}_m, T)$ gravity:

$$M = M_0 - \beta \frac{\mathcal{R}}{2} \psi(\mathcal{R}), \text{ where } M_0 = \frac{\mathcal{R}}{2} (1 - e^{-W(r)}).$$
 (61)

This formulation set forth the contributions from stand-

ard $f(\mathcal{R}, \mathcal{L}_m, T)$ gravity from those introduced by the gravitational decoupling. The compactness factor [91] for $f(\mathcal{R}, \mathcal{L}_m, T)$ gravity due to MGD approach can be written

$$u^{eff} = \frac{M}{\mathcal{R}} = u_0 - \frac{\beta}{2}\psi(\mathcal{R}), \text{ where } u_0 = \frac{M_0}{\mathcal{R}}.$$
 (62)

Due to the impact of compactness u^{eff} , the surface gravitational redshift z_s is also influenced by the decoupling process. Thus, the modified surface redshift z_s in the context of MGD for $f(\mathcal{R}, \mathcal{L}_m, T)$ gravity is expressed [92] as follows:

$$z_s = \left(1 - 2u_0 + \beta\psi(\mathcal{R})\right)^{-1/2} - 1,\tag{63}$$

Following the discussion on mass, redshift, and compactness under the gravitational decoupling effect, a few key points can be outlined form the graphical analysis:

• First, it is possible to achieve mass expansion using MGD technique [93] within $f(\mathcal{R}, \mathcal{L}_m, T)$ gravity. As seen from Eq.(61), if the second term is positive, the overall mass increases. In our case, this is possible for negative values of the interaction parameter β . As the mass increases, both the redshift (z_s) and compactness (u) also increase. Various authors have previously achieved simil-

ar results, as seen in [94], where mass expansion is observed for negative β , while in [95, 96], the authors reported mass expansion for positive coupling parameter values. Tables 3 and 4 displays the values of mass, redshift, and compactness with and without the coupling effect for both negative and positive β values across seven star candidates, respectively. It is noted that mass increases only for positive β values, whereas for negative β , the modified mass is less than the original. Additionally, the critical values of the adiabatic index using Eq.(58) for modified mass using the MGD approach are shown in the table for all stars, and it is observed that the value is greater than 4/3 in both cases (positive and negative β values), confirming the stable trend of the proposed model within the realm of $f(\mathcal{R}, \mathcal{L}_m, T)$ gravity. Moreover, Figures (10) and (11) show the plots of modified mass, redshift, and compactness for both cases.

• Secondly, the modified compactness due to MGD

results in greater compactness compared to the compactness without this effect. Our findings are also consistent with the Buchdahl limits [97] for isotropic fluids $(u \le 4/9)$ and anisotropic fluids $(u \le 0.30)$, which is crucial for establishing a physically acceptable model.

Table 5 presents a clear comparative analysis of various anisotropic stellar models developed within different modified gravity frameworks. It highlights the distinct features of each model and illustrates how the present study based on Class-I solutions within the Minimal Geometric Deformation (MGD) approach relates to and extends previous works. By adopting a more generalized gravitational theory, namely $f(R, L_m, T)$, which encompasses earlier special cases, and by utilizing realistic values of mass and radius of compact stars, the model offers a physically consistent anisotropic extension of an initially isotropic seed solution. This comparative framework emphasizes the novelty and physical viability of the

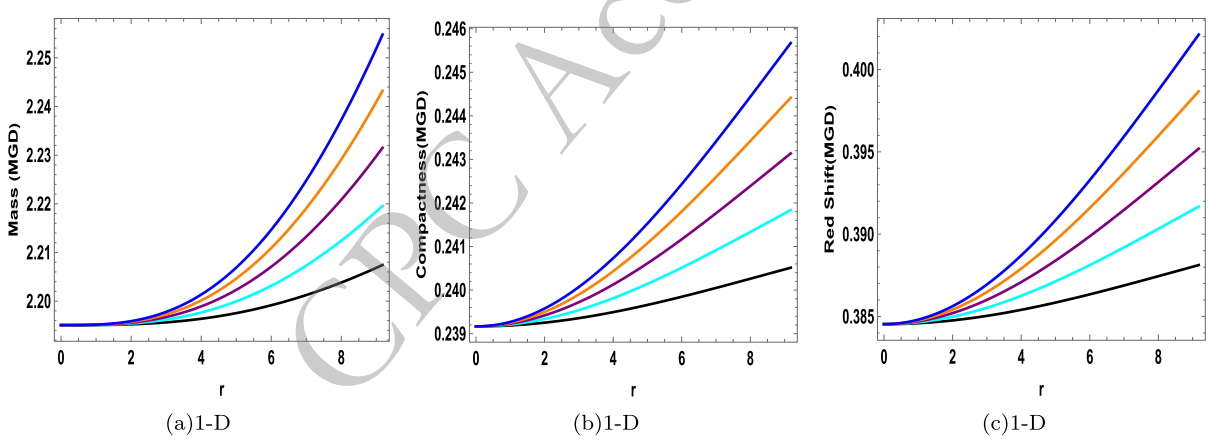


Fig. 10. (color online) For the compact star Cen X-3 ($\mathcal{M}/\mathcal{M}_{\odot} = 1.49$, $\mathcal{R} = 9.178$), the plots show how the mass function, compactness, and redshift vary with the radial coordinate r. The variation is considered for some variations of β : $\beta = -0.1$ (\blacksquare), $\beta = -0.2$ (\blacksquare), $\beta = -0.3$ (\blacksquare), and $\beta = -0.5$ (\blacksquare). In all plots, the parameters are set to $\beta = 0.01$, $\alpha = 0.03$, $\alpha = 0.09$, and $\alpha = 0.09$, and $\alpha = 0.09$.

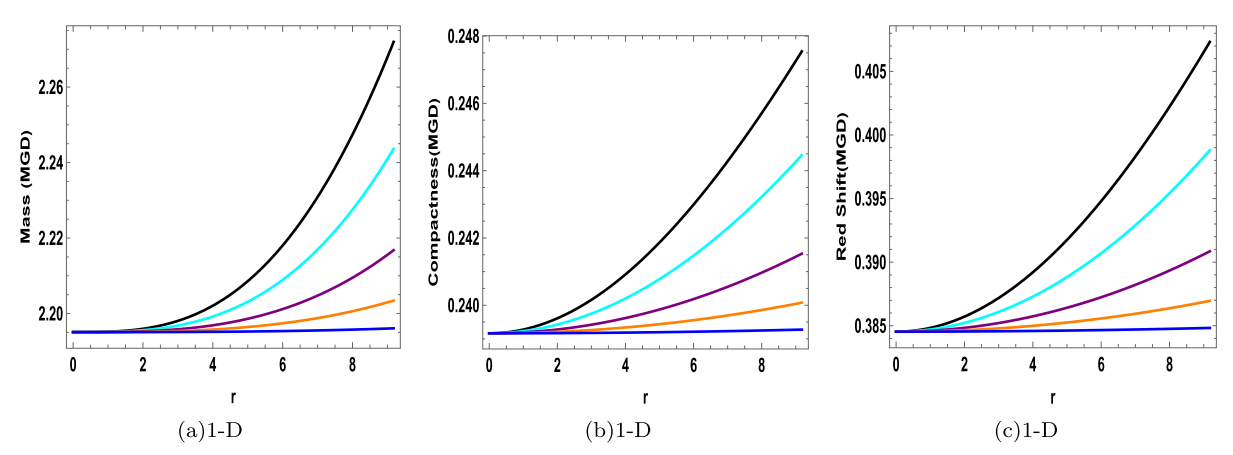


Fig. 11. (color online) For the compact star Cen X-3 ($M/M_{\odot} = 1.49$, $\mathcal{R} = 9.178$), the plots show how the mass function, compactness, and redshift vary with the radial coordinate r. The variation is considered for some values of n: n = 0.5 (\blacksquare), n = 1 (\blacksquare), n = 1.5 (\blacksquare), n = 1.5 (\blacksquare), and n = 3 (\blacksquare). In all plots, the parameters are set to n = 0.1, n = 0.0003, n = 0.0009, and n = 0.0003, and n = 0.0003, n = 0.0003, n = 0.0009, and n = 0.0003, n = 0.0009, and n = 0.0003.

Gravity theory	Metric Anstaz	Matter Configuration	Stability & Features
$f(\mathcal{R},T)[98]$	Krori-Barua metric	Anisotropic fluid	Physically acceptable; matched with Schwarzschild
f(X,T)[98]	THOIT Burda metre	i insotropie riara	exterior; consistent graphs for real stars
$f(\mathcal{T})[99]$ gravity	Krori-Barua metric	Anisotropic fluid	Regular and stable; consistent with 4U 1820-30, Her X-1,
) () [)] Biuvity		1	and SAX J1808.4-3658; surface redshift analyzed
$f(\mathcal{O}, \mathcal{C}, T) = \mathcal{O} + \alpha T \mathcal{C}$ [100]	Numerical (non-KB)	Anisotropic quark matter; MIT	Mass–radius relation, adiabatic index, sound speed; α
$f(\mathcal{R}, \mathcal{L}_m, T) = \mathcal{R} + \alpha T \mathcal{L}_m[100]$	rumericai (non RD)	bag model	constrained using observational data
$f(\mathcal{R}, \mathcal{L}_m, T)$	Class 1 ambadding: MCI	Anisotropic fluid; radial metric	Well-behaved energy density/pressures; negative β yields
$f(N, \mathcal{L}_m, \Gamma)$	$f(N, \mathcal{L}_m, T)$ Class-Telliocading, IVIOI		higher mass; stability via TOV and Herrera cracking
Present Work	approach	deformation	condition

Table 5. omparison of anisotropic stellar models in various modified gravity frameworks.

present model within the broader context of modified gravity theories.

It is important to note that mass–radius (M–R) curves provide the most direct diagnostic of stellar configurations. In the present analysis, we have fixed the stellar mass and adopted assumed radii to examine physical behaviour. However, previous works in GR [101], f(R) gravity [102–104], and f(R,T) gravity [105–110], as well as more recent studies in $f(R,\mathcal{L}_m,T)$ models [111, 112], have shown that matter–geometry couplings significantly shift M–R relations. The compactness and redshift trends we obtain are qualitatively consistent with these results. Our approach differs by employing the generalized $f(R,\mathcal{L}_m,T)$ framework together with the Minimal Geometric Deformation technique.

Unraveling the true mass and radius of pulsars remains one of the central challenges in compact star astrophysics. Despite notable observational progress, these parameters still involve uncertainties due to the extreme physical conditions and complex matter interactions inside such objects. In this work, we propose a refined modeling strategy within the extended $f(R, \mathcal{L}_m, T)$ gravity framework to better capture the structure of pulsars under modified gravitational dynamics. To connect our theoretical model with observational reality, we have benchmarked it against reliable data from well-studied pulsars, including Her X-1 [71], LMC X-4 [72], Cen X-3 [73], 4U 1538-52 [74], Vela X-1 [75], PSR J1614-2230 [76], and PSR J0740+6620 [77]. These compact objects span a wide mass range and provide a robust testing ground for assessing the predictive power and flexibility of our model.

In future work, we plan to extend this analysis by numerically constructing explicit M–R sequences in $f(R, \mathcal{L}_m, T)$ gravity and benchmarking them directly against GR, f(R), and f(R, T) predictions, thereby offering deeper insights into the physics of ultra-dense stars.

V. CONCLUSION

In this research, we employed the Minimal Geometric Deformation (MGD) approach for gravitational decoupling within the framework of $f(\mathcal{R}, \mathcal{L}_m, T)$ gravity to

construct anisotropic compact star models based on a class-1 embedding spacetime. In the literature, this method has proven highly effective for developing interior solutions of self-gravitating systems, enabling the investigation of gravitational effects from various perspectives within spherically symmetric configurations. In the present work, we utilized Ovalle's gravitational decoupling technique [96] along with the MGD approach in the context of $f(\mathcal{R}, \mathcal{L}_m, T)$ gravity to formulate physically viable models of compact stellar objects with anisotropic pressure. Within this framework, one of the metric potentials was deformed, introducing an additional gravitational source that decoupled the original field equations into two separate systems. The first system corresponds to the standard perfect fluid Einstein equations described by $T_{\mu\nu}$, while the second governs the anisotropic source $\vartheta_{\mu\nu}$, forming a quasi-Einstein system. Notably, these two sources interact solely through gravitational interaction, without any direct energy exchange. We introduced the deformation by modifying the radial component of the metric through an appropriate choice of the function $\psi(r)$ [70, 94], ensuring the regularity in the metric functions and all essential physical parameters throughout the stellar interior. It is important to note that setting the coupling parameter $\beta = 0$ recovers the original field equations of the theory. Additionally, the constants A, B, and cwere determined by matching the interior solution to the exterior Schwarzschild geometry.

The effective radial pressure $p_r^{\rm eff}=0$ at the boundary, derived from the second fundamental form of the junction conditions, incorporates both the isotropic pressure p_r and the deformation function $\psi(r)$, which arises due to the additional source $\tilde{\theta}_{\mu\nu}$. Using realistic observational data, we have determined the constants A, B, and c for seven compact stellar candidates: Her X-1, Cen X-3, LMC X-4, Vela X-1, PSR J1614-2230, 4U 1608-52, and PSR J0740+6620, with the corresponding results presented in Tables 1 and 2. The compact star Cen X-3 has been chosen for graphical examination because its radius ($\mathcal{R}=9.178$) lies in an optimal range that allows comprehensive illustration of all physical parameters, including energy density, pressure profiles, anisotropy, energy conditions, and equilibrium forces. Larger radii were re-

quired to exhibit the full behavior of these quantities, making Cen X-3 a suitable candidate. For graphical analysis, we evaluated the physical behavior of the model under two distinct scenarios: one involving variations in the coupling parameter β , and the other involving changes in the deformation parameter n, both using Cen X-3 as the reference model. In the following, we summarize the key conclusions derived from this study:

- Figures (1(a)) and (1(b)) showed how gravitational decoupling affects the metric potentials for both scenarios, using Cen X-3 star's observational data and constants A = -0.0403881, B = -0.0306402, and C = 0.00454612. The metric potentials have clearly indicated positive and monotonically decreasing behavior within the star before diminishing at the boundary, fostering our model's regularity and stability.
- Figures (2(a)), (2(b)), (2(c)), and (3(a)) have shown positive, non-singular, and monotonically decreasing behavior of energy density and pressures inside the stellar structure. It has been noticed that radial pressure vanishes at the star's surface, validating the model's physical consistency.
- Figures (4(c)) and (5(c)) depicted the trend of anisotropy profile, which is positive increasing function of r and turns out to be zero at the boundary (indicating that the radial and tangential pressures are equal there).
- Figures (3(b)) and (3(c)) have illustrated negative and monotonically declining gradients of energy density and pressures, which satisfied the required constraint of vanishing at r = 0 given in Eq.(50), and hence assured the model's physical validity.
- Furthermore, Figures (4(a)), (4(b)), (5(a)), and (5(b)) have shown the energy condition inequalities, which demonstrated that all energy bounds (NEC, SEC, DEC, and WEC) have been validated throughout the stellar interior given in Eq.(51).
- Figure (6) has depicted the model's hydrostatic equilibrium given by Eq.(52), which is derived from the balancing of hydrostatic force (F_h) , gravitational force (F_g) , anisotropic force (F_a) , and the modified force (F_m) due to $f(\mathcal{R}, \mathcal{L}_m, T)$ gravity. This ensures that the forces counter balance one another, preventing the gravitational collapse and confirming the model's stability.
- The EoS, as shown in the Figures (7(a)) and (7(b)), indicated that all values are between 0 and 1.
- Also, the speed of sounds $(v_r^2 \& v_t^2)$ remained lower than the speed of light throughout the stellar interi-

or as shown in Figures (8) and (9(a)). This clearly meets the criteria for causality and stability.

• Furthermore, the adiabatic index surpasses the essential value of 4/3, guaranteeing the static stability. Furthermore, Herrera's cracking condition has been met.

Clearly, the TOV equation has held true in the re-designed framework, indicating that our solutions reflect physically viable, stable, and equilibrium compact star models. Tables (III) and (IV) show the mass, redshift, and compactness values, with and without minimal geometric deformation. Notably, we have observed that negative values of the coupling parameter β allow for greater mass packing, as evidenced by the increased values of mass, redshift, and compactness compared to the un-deformed case. Figure (10) clearly demonstrated that these values rise monotonically with r, reaching a highest value at the star's surface for $\beta = -0.5$. Figure (11) showed how varying n affects these parameters, with the maximum values occurring at n = 3 for $\beta = -0.2$.

This work concludes by highlighting the important effects of gravitational decoupling via the MGD technique on the compactness ($u = M/\Re$) and total mass of compact star models. When β takes negative values, the additional gravitational source induced and governed by the coupling parameter β enables higher mass confinement within the stellar structure. This realization underscores the flexibility and strength of the MGD approach in constructing stable and physically consistent compact star solutions with anisotropic pressures and extended gravitational influences.

In particular, our findings differ from previous studies in other modified gravity models, as shown in the comparative Table 5, where such significant variation in mass due to deformation and coupling has not been reported within the context of $f(\mathcal{R}, \mathcal{L}_m, T)$ gravity. Specifically, the simultaneous increase and decrease in mass and compactness with different β values is a novel result in this theory, revealing new physical insights that have not been previously explored. Table 5 presents a comparative summary of our model with other recent works, clearly emphasizing the theoretical and physical advancements achieved. In f(R) theory, Sharif and Aslam [113] explored anisotropic spherical symmetric solutions through extended gravitational decoupling approach. By considering Starobinsky model of f(R) gravity along with Krori-Barua metric potential, two sorts of solutions have been presented. It has been shown that one of the two developed models exhibited locally unstable conduct when different values of coupling parameter are used. In another study [58], authors investigated the construction of anisotropic static spheres by using the metric potentials of Tolman V solution and minimal geometric deformation scheme in $f(R,T^2)$ gravity. Solutions were obtained by

imposing three different constraints, it has been found that first two models are physically viable and stable only when small choices of decoupling parameter are taken. In present work, we have considered linear $f(R, L_m, T)$ model and it has been found that for all choices of β parameter, the obtained model exhibited stable and physically valid behavior. In a recent work, Singh et al. [65] have explored anisotropic compact star configurations for self-gravitating structure through minimal geometric deformation scheme along with of embedding class-1 spacetime in GR framework. They performed the graphical analysis by considering different variations of coupling parameter α and n. It is shown that all physical characteristics are satisfied when positive values of α are considered. Our work is an extension of this work by involving curvature-

matter coupling and the results obtained are quite similar. Using same metric potential along with gravitational coupling approach, Hira et al. [64] modeled some compact stellar structures in Rastall theory. Through graphical analysis of different measures, physically valid models are obtained when positive coupling parameter values are taken, and our obtained results are also in agreement with their findings.

The effective implementation of this technique within the framework of $f(\mathcal{R}, \mathcal{L}_m, T)$ gravity offers promising new directions for the study of compact stars in alternative gravity theories and enhances our understanding of the internal composition and evolution of dense astrophysical objects.

References

- [1] J. M. Lattimer, M. Prakash, Phys. Rev. Lett. **94**, 111101 (2005)
- [2] B. P. Abbott, R. Abbott, T. D. Abbott, et al., Phys. Rev. Lett. 119, 161101 (2017)
- [3] K. Akiyama, A. Alberdi, W. Alef, *et al.*, Astrophys. J. Lett. **875**, L1 (2019)
- [4] S. Perlmutter, G. Aldering, G. Goldhaber, et al., Astrophys. J. 517, 565 (1999)
- [5] A. G. Riess, A. V. Filippenko, P. Challis, et al., Astron. J. 116, 1009 (1998)
- [6] D. N. Spergel, L. Verde, H. V. Peiris, et al., Astrophys. J. Suppl. Ser. 148, 175 (2003)
- [7] E. Komatsu, J. Dunkley, M. R. Nolta, et al., Astrophys. J. Suppl. Ser. 180, 330 (2009)
- [8] S. W. Hawking, R. Laflamme, Phys. Lett. B 209, 39 (1988)
- [9] A. Narimani, N. Afshordi, D. Scott, J. Cosmo. Astropart. Phys. 2014, 049 (2014)
- [10] J. S. Farnes, Astron. Astrophys. **620**, A92 (2018)
- [11] T. P. Sotiriou, V. Faraoni, Rev. Mod. Phys. 82, 451 (2010)
- [12] S. Capozziello, M. De Laurentis, Phys. Rep. **509**, 167
- [13] K. Hayashi, T. Shirafuji, Phys. Rev. D 19, 3524 (1979)
- [14] E.E. Flanagan, E. Rosenthal, Phys. Rev. D, **75**: 124016 (2007).
- [15] J. B. Dent, S. Dutta, E. N. Saridakis, J. Cosmol. Astropart. Phys. 2011, 009 (2011)
- [16] K. Bamba, C-Q Geng, C-C Lee, et al., J. Cosmo. Astropart. Phys. 2011, 021 (2011)
- [17] M. Zubair, F. Kousar, R. Saleem, Chin. J. Phys. **65**, 355 (2020)
- [18] F. Kousar, R. Saleem, M. Zubair, Adv. High Energy Phys. 2018, 3085761 (2018)
- [19] M. Zubair, F. Kousar, S. Waheed, Can. J. Phys. 97(8), 880 (2019)
- [20] N. M. García, F. S. N. Lobo, J. P. Mimoso, *et al.*, J. Phys. Conf. Ser., **314**: 012056 (2011).
- [21] S. K. Maurya, A. Errehymy, D. Deb, et al., Phys. Rev. D 100, 044014 (2019)
- [22] M. Caruana, G. Farrugia, J. L. Said, Eur. Phys. J. C 80, 640 (2020)

- [23] E. Gudekli, M. Zubair, M. J. Kamran, *et al.*, Int. J. Geom. Meth. Mod. Phys. **19**(4), 2250056 (2022)
- [24] R. Saleem, M. I. Aslam, M. Zubair, Eur. Phys. J. Plus **136**(10), 1078 (2021)
- [25] M. Zubair, A. Ditta, S. Waheed, et al., Chin. J. Phys. 77, 1827 (2022)
- [26] S. K. Maurya, J. Kumar, S. Kiroriwal, JHEAP **44**, 194 (2024)
- [27] S. K. Maurya, A. Errehymy, Y. Saginayev, *et al.*, Phys. Dark Univ. **49**, 101977 (2025)
- [28] S. K. Maurya, K. N. Singh, M. Govender, et al., Astrophys. J. Suppl. 269(2), 35 (2023)
- [29] L. V. Jaybhaye, R. Solanki, S. Mandal, et al., Phys. Lett. B 831, 137148 (2022)
- [30] Z. Haghani, T. Harko, Eur. Phys. J. C 81, 615 (2021)
- [31] M. Zubair, S. Waheed, Q. Muneer, *et al.*, Fortsch. Phys. **71**(8), 2300018 (2023)
- [32] C. E. Mota, J. M. Z. Pretel, C. O. V. Flores, Eur. Phys. J. C 84, 673 (2024)
- [33] G. G. L. Nashed, W. El Hanafy, J. Cosmo. Astropart. Phys. 09, 038 (2023)
- [34] G. G. L. Nashed, S. Capozziello, Eur. Phys. J. C 84, 521 (2024)
- [35] G. G. L. Nashed, Astrophysical Journal **950**(2), 129 (2023)
- [36] A. Das, F. Rahaman, B. K. Guha, et al., Eur. Phys. J. C 76, 654 (2016)
- [37] J. Kumar, H. D. Singh, A. K. Prasad, Phys. Dark Univ. 34, 100880 (2021)
- [38] A. K. Yadav, M. Mondal, F. Rahaman, Pramana J. Phys. **94**, 90 (2020)
- [39] D. Taser, S. S. Dogru, Astrophys. Space Sci. 368(6), 49 (2023)
- [40] J. Ovalle, R. Casadio, R. da Rocha, et al., Eur. Phys. J. C 78, 122 (2018)
- [41] L. Randall, R. Sundrum, Phys. Rev. Lett. **83**, 4690 (1999)
- [42] R. Casadio, J. Ovalle, R. da Rocha, Class. Quantum Gravit. 32, 215020 (2015)
- [43] J. OVALLE, Int. J. Mod. Phys. D 18, 837 (2009)
- [44] R. Casadio, J. Ovalle, Phys. Lett. B **715**, 251 (2012)
- [45] J. Ovalle, Phys. Lett. B **788**, 213 (2019)
- [46] R. da Rocha, Eur. Phys. J. C 77, 355 (2017)
- [47] R. Casadio, P. Nicolini, R. da Rocha, Class. Quantum Gravit. 35, 185001 (2018)

- [48] C. las Heras, P. León, Fortschritte der Phys., **66**: 070036 (2018).
- [49] M. Estrada, F. Tello-Ortiz, Eur. Phys. J. Plus 133, 453 (2018)
- [50] M. Sharif, S. Saba, Eur. Phys. J. C 78, 921 (2018)
- [51] E. Morales, F. Tello-Ortiz, Eur. Phys. J. C 78, 618 (2018)
- [52] M. Estrada, R. Prado, Eur. Phys. J. Plus 134, 168 (2019)
- [53] E. Contreras, P. Bargueno, Eur. Phys. J. C 78, 558 (2018)
- [54] H. Azmat, M. Zubair, Phys. Dark Univ. **37**, 101049 (2022)
- [55] H. Azmat, R. Khalid, M. Zubair, et al., Commun. Theor. Phys. 77(6), 065401 (2025)
- [56] H. Azmat, F. Tello-Ortiz, M. Zubair, et al., Phys. Scripta 98(1), 015010 (2022)
- [57] S. K. Maurya, F. Tello-Ortiz, Phys. Dark Univ. 27, 100442 (2020)
- [58] M. Sharif, S. Iltaf, Physica Scripta 97, 075002 (2022)
- [59] S. K. Maurya, A. Errehymy, B. Dayanandan, et al., JHEAP 45, 46 (2025)
- [60] S. K. Maurya, A. Errehymy, K. N. Singh, et al., J. Cosmol. Astropart. Phys. 04, 004 (2025)
- [61] H. Azmat, M. Zubair, Eur. Phys. J. Plus **136**(1), 112 (2021)
- [62] S. Sahlu, A. H. A. Alfedeel, A. Abebe, Eur. Phys. J. C 84(9), 982 (2024)
- [63] K. Lake, Phys. Rev. D 67, 104015 (2003)
- [64] H. Sohail, A. Ditta, I. Mahmood, et al., Eur. Phys. J. Plus 139(8), 695 (2024)
- [65] K. N. Singh, S. K. Maurya, M. K. Jasim, et al., Eur. Phys. J. C 79(10), 851 (2019)
- [66] D. M. Pandya, B. Thakore, R. B. Goti, et al., Astrophys. Space Sci. 365(2), 30 (2020)
- [67] S. N. Pandey, S. P. Sharma, Gen. Relativ. Gravit. 14, 113 (1982)
- [68] M. Estrada, R. Prado, Eur. Phys. J. Plus 134, 168 (2019)
- [69] E. Morales, F. Tello-Ortiz, Eur. Phys. J. C 78, 841 (2018)
- [70] K. N. Singh, S. K. Maurya, M. K. Jasim, et al., Eur. Phys. J. C 79, 851 (2019)
- [71] M. K. Abubekerov, E. A. Antokhina, A. M. Cherepashchuk, *et al.*, Astron. Rep. **52**, 379 (2008)
- [72] M. L. Rawls, J. A. Orosz, J. E. McClintock, et al., Astrophys. J. 730, 25 (2011)
- [73] S. Naik, B. Paul, Z. Ali, Astrophys. J. **737**, 79 (2011)
- [74] F. E. Marshall, L. Angelini, IAU Circ. **6331**, 1 (1996)
- [75] M. L. Rawls, J. A. Orosz, J. E. McClintock, et al., Astrophys. J. 730, 25 (2011)
- [76] Z. Arzoumanian, et al., Astrophys. J. Suppl. 235(2), 37 (2018)
- [77] M. Miller, F. K. Lamb, A. Dittmann, et al., APJL 887, L24 (2019)
- [78] A. Chanda, S. Dey, B. C. Paul, Eur. Phys. J. C **79**, 502 (2019)
- [79] B. V. Ivanov, Phys. Rev. D 65, 104001 (2002)
- [80] S. W. Hawking, G. F. R. Ellis, *The Large Scale Structure of Space-Time*, (Cambridge University Press, 2023).
- [81] R. Bousso, Rev. Mod. Phys. 74, 825 (2002)
- [82] S. Das, F. Rahaman, L. Baskey, Eur. Phys. J. C 79, 853

(2019)

[97]

- [83] A. Di Prisco, L. Herrera, V. Varela, Gen. Relativ. Gravit. 29, 1239 (1997)
- [84] L. Herrera, Phys. Lett. A 165, 206 (1992)
- [85] H. Abreu, H. Hernandez, L. A. Nunez, Classic. Quantum Gravit. 24, 4631 (2007)
- [86] H. Andreasson, Commun. Math Phys. 288, 715 (2009)
- [87] S. Chandrasekhar, Astrophys. J. **140**, 417 (1964)
- [88] D.D. Doneva and S.S. Yazadjiev, Phys. Rev. D **85**, 124023 (2012)
- [89] H. O. Silva, C. F. B. Macedo, E. Berti, et al., Class. Quantum Gravit. 32, 145008 (2015)
- [90] C. C. Moustakidis, Gen. Relativ. Gravit. 49, 68 (2017)
- [91] M. K. Mak, T. Harko, Proc. R. Soc. London Ser. A Math Phys. Eng. Sci. 459, 393 (2003)
- [92] C. G. Bohmer, T. Harko, Class. Quantum Gravit. 23, 6479 (2006)
- [93] C. Arias, F. Tello-Ortiz, E. Contreras, Eur. Phys. J. C 80, 463 (2020)
- [94] H. Sohail, A. Ditta, I. Mahmood, et al., Eur. Phys. J. Plus 139, 695 (2024)
- [95] S. Chakraborty, S. SenGupta, J. Cosmo. Astropart. Phys. 2018, 032 (2018)
- [96] F. Tello-Ortiz, Eur. Phys. J. C **80**, 413 (2020)
 - H. A. Buchdahl, Phys. Rev. 116, 1027 (1959)
- [98] M. F. Shamir, Z. Asghar, A. Malik, Fortschritte Der Physik 70, 12 (2022)
- [99] G. Abbas, A. Kanwal, M. Zubair, Astrophys. Space Sci. 357(2), 109 (2015)
- [100] T. Tangphati, I. Sakalli, A. Banerjee, et al., Chin. Phys. C 49(2), 025110 (2025)
- [101] S. K. Maurya, M. K. Jasim, A. Errehymy, *et al.*, Eur. Phys. J. C **85**(3), 321 (2025)
- [102] R. Kumar, S. K. Maurya, Y. Sekhmani, et al., Nucl. Phys. B 1018, 116984 (2025)
- [103] M. Zubair, G. Abbas, Astrophys. Space Sci. **361**, 342 (2016)
- [104] G. G. L. Nashed, S. Capozziello, Eur. Phys. J. C 84, 521 (2024)
- [105] A. Errehymy, Y. Khedif, G. Mustafa, et al., Chin. J. Phys. 77, 1502 (2022)
- [106] P. H. R. S. Moraes, J. D. V. Arbañil, M. Malheiro, JCAP 06, 005 (2016)
- [107] K. N. Singh, S. K. Maurya, A. Errehymy, et al., Phys. Dark Univ. 30, 100620 (2020)
- [108] K. N. Singh, A. Errehymy, F. Rahaman, et al., Chin. Phys. C 44(10), 105106 (2020)
- [109] M. Rahaman, K. N. Singh, A. Errehymy, et al., Eur. Phys. J. C 80(3), 272 (2020)
- [110] K. N. Singh, A. Errehymy, F. Rahaman, et al., Chin. Phys. C 44(10), 105106 (2020)
- [111] J. A. S. Fortunato, P. H. R. S. Moraes, E. Brito, et al., Phys. Dark Univ. 48, 101893 (2025)
- [112] C. E. Mota, J. M. Z. Pretel, C. O. V. Flores, Eur. Phys. J. C 84, 673 (2024)
- [113] M. Sharif, M. Aslam, Eur. Phys. J. C 81, 641 (2021)